공학석사 학위논문

Numerical Investigation of Confluence Flows with Various Discharge Ratios and Junction Angles

유량비 및 합류각에 따른 합류부 흐름에 관한 수치적 연구

2020 년 8 월

서울대학교 대학원

건설환경공학부

김 지 환

Abstract

Confluent flow is one of the most common hydrodynamic phenomena. Thus, it has been studied numerically as well as experimentally in various fields of engineering by many researchers. However, most numerical studies were carried out in two dimensions under limited conditions of discharge ratios or junction angles and not comprehensively validated.

Therefore, this study conducted the three-dimensional numerical investigation of the effects of the discharge ratio and junction angle to flow characteristics associated with the primary and secondary flow patterns, separation zones, water depth, bed shear stress, turbulent kinetic energy, etc. in various confluences using open source CFD software OpenFOAM. The numerical results have been reasonably validated against the experimental data of Gurram (1997) and Shumate (1998). It showed a good agreement between the simulation results and observations. It was verified that the separation zone, the maximum velocity, maximum turbulent kinetic energy, maximum bottom shear stress, and the depth depression zone, and depth ratio variation increased while the discharge ratio and junction angle increased.

Multiple Linear Regression (MLR) models from the simulation results and the goodness-of-fit and estimation were modelled and validated with the adjusted R-squared values and the MSE values. Moreover, the sensitivity analysis using the sum of the partial derivatives verified that the separation zone

varied more sensitively to the junction angle, whereas the other characteristics changed more sensitively to the discharge ratio.

However, the number of simulation cases was not enough for comprehensive validation and the effects of the width and depth of the channels were not considered due to the high computational time. Thus, it is necessary to conduct a greater number of simulations with different discharge ratios, junction angles, channel width, and depth to prove the validity of the simulation results and apply the mathematical models to different geometries.

Keywords: Confluent flow, 3D numerical model, Discharge ratio, Junction angle, OpenFOAM, Separation zone, Secondary flow.

Student Number: 2018-21243

Table of Contents

List of Figures

List of Tables

Nomenclature

Latin Symbols

Letter	Description
b_s	Width of the separation zone
E	Wall smoothness coefficient
e	Error term
$\overline{f_i}$	External force
g	Acceleration of gravity
h	Water depth
h_d	Downstream water depth
I	Turbulence intensity
K	The number of parameters
k	Turbulent kinetic energy
L_s	Length of the separation zone
n	The number of data points
p	Pressure
$\overline{p}$	Mean pressure
q^*	Discharge ratio
Q_b	Flowrate of a branch channel
Q_m	Flowrate of a main channel

S	Invariant measure of the strain rate
$SS_{residuals}$	Residual sum of squares
SS_{total}	Total sum of squares
t	Time
u	Velocity component in x-direction
u^*	Non-dimensional u
$\overline{u_i}$	Mean velocity
u_τ	Friction velocity
u_τ^{vis}	Friction velocity for viscous layers
$u_\tau^{\log}$	Friction velocity for logarithmic layers
v	Velocity component in y-direction
v^*	Non-dimensional v
w	Velocity component in z-direction
w^*	Non-dimensional w
$\overline{x}$	Mean of x
x_i	Explanatory variable
x^*	Non-dimensional x
Y_i	Observed values
$\widehat{Y}_i$	Expected values
$\overline{y}$	Mean of y

y^+	Dimensionless wall distance
y^*	Non-dimensional y
y_i	Dependent variable
z^*	Non-dimensional y

Greek Symbols

Letter	Description
α	Fraction of volume
β_0	y-intercept
β_p	Slope coefficients
ε	Turbulent dissipation
κ	Von-Karman constant
ν	Kinematic viscosity
ν_t	Turbulent viscosity
ρ	Density of water
ρ_{xy}	Correlation between x and y
ω	Turbulent specific dissipation rate
ω_{vis}	specific dissipation rates for viscous layers
ω_{log}	specific dissipation rates for logarithmic layers
δ_{ij}	Kronecker delta

Chapter 1. Introduction

1.1 Introduction

Confluent flow or combining flow is a flow where two or more than two flows meet together as shown in Figure 1 and it is one of the most common hydrodynamic phenomena in several hydraulic systems around the world such as rivers, open channels, canals and so on. The confluent flow has been studied in a variety of fields including engineering, natural science, and even social science and humanities. For instance, Best (1988) and Liu et al. (2015) have found out that the angles and discharge ratios of river channel confluences affect dramatic changes in flow, bed morphology, and sediment discharge which can result in disturbance of flows (water, sediment, effluent, and nutrition) and damage of structures. The experiments in different angles and discharge ratios revealed that the bed was eroded around the confluence zones and the shapes and sizes of them increased, the bed morphology change increased, and the sediment loads became segregated more as the confluence angles and discharge ratios increased. In addition, Rice et al (2008) stated that confluences are ecologically important places that impact habitats of creatures due to the recruitment of the water, sediment, and organic substances. Furthermore, the confluence flow can result in fatal disasters. The flood in 2018, Japan caused by a backwater effect of a confluence flow killed at least 48 residents and submerged 12 square kilometers. The water level of the branch stream rose too high since the branch stream was blocked by the mainstream during the heavy

rain. The increased flow from the branch stream breached the banks and submerged the riverside areas. Thus, it is highly essential to understand the flow structure and phenomena of the confluent flow.

The flow phenomenon varies with the discharge ratios, junction angles, Froude number, channel widths, and water depths. Thus, a number of studies have been conducted to investigate the flow patterns through numerous experiments at open channels with different specification (Taylor, 1944; Anwar, 1955; Webber & Greated; 1966; Lin and Soong, 1979; Best and Reid, 1984; Ramamurthy et al., 1988; Biron et al., 1996; Gurram et al., 1997, Hsu et al., 1998; Shumate, 1998; Choi et al., 2003; Choi et al., 2004; Beharnagi et al., 2005; Choi and Kim, 2006; Qing-Yuan et al., 2007; Wang et al., 2007; Biswal et al., 2010; Mignot et al., 2012; Birjukova et al., 2012; Kwak and Rhee, 2012; Lee, 2013; Yoshimura et al., 2015; Coelho, 2015; Biswal et al., 2016; Creelle et al., 2016; Schindfessel, 2016; Yuan et al., 2016; Penna et al.,2018).

Furthermore, a variety of numerical studies with Computation Fluid Dynamics (CFD) have been carried out as well as experimental studies and they were attempted to be validated against the experimental results which described above since there are numerous advantages of CFD against experiments (Choi and Kang, 1993; Bradbrook et al., 2001; Huang et al., 2002; Biron et al., 2004; Choi et al., 2004 & 2005; Sivakumar et al., 2004; Cho et al., 2005; Ahn et al., 2006; Cho, 2007; Jang et al., 2007; Shakibainia et al., Kim et al., 2009; 2010; Bonakdari et al., 2011; Song, 2011; Mignot et al., 2012; Ghostine et al., 2012;

Seo and Park, 2013; Yang et al., 2013; Ahn et al., 2014; Brito et al., 2014; Schindfessel et al., 2015; Yoshimura et al., 2015; Sharifipour, 2015; Schindfessel et al., 2016, Kim et al., 2016; Jang and Ji, 2017; Luo et al., 2018; Penna et al.,2018; Ramos et al., 2019). The main reasons for numerical studies overcoming experimental studies are that it is more cost-effective, there is less limit than experiments, the result is not affected by the research sites, and it is able to measure certain values which are not possible for some experiments. Thus, it is necessary to implement CFD techniques to investigate the certain phenomenon of confluent flow.

However, most numerical studies were two dimensional and conducted within only single or limited specifications. Furthermore, they were validated against limited specifications.

Therefore, this study conducted a three-dimensional investigation of the effects of discharge ratios and junction angles on flows characteristics associated with the primary and secondary flow patterns, shapes of separation zones, water depth, bed shear stress, kinetic energy, etc. at various confluences and validate the numerical results against the experimental results in order to implicate the result to other study fields such as bed morphology, sediment transport, ecology and so forth. In addition, mathematical models were developed by Multiple Linear Regression to provide the simple estimation method of the flow characteristics and the sensitivity analysis using the sum of the partial derivatives was conducted to investigate the sensitivity of the

discharge ratios and junction angles to the flow characteristics.

Figure 1. Confluence of the waters in Manaus, Brazil

1.2 Necessity and Objective

The confluence flows are important for diverse fields of research since they affect a number of aspects as mentioned above. Thus, they have been studied experimentally as well as numerically by many researchers.

However, most studies of them were carried out about only right-angled junction flows against discharge ratios or Froude numbers, but not many studies on different angles and their effects. Especially there were several numerical studies with a single junction angle but not many in different junction angles (Huang et al., 2002; Sivakumar et al., 2004; Cho et al., 2005; Bonakdari et al., 2011; Mignot et al., 2012; Yang et al., 2013; Brito et al., 2014; Schindfessel et al., 2015; Yoshimura et al., 2015; Sharifipour, 2015; Schindfessel et al., 2016; Ramos et al., 2019). Even some numerical studies with different angles were not validated against any experiment result or only with a single angle of experiment results (Bradbrook et al., 2001; Biron et al., 2004; Shakibainia et al., 2010; Luo et al., 2018; Penna et al., 2018). In addition, most multiple angle numerical studies were conducted in one or two dimensions without any validation, even all the flow characteristics should be developed and expressed in three dimensions. Furthermore, most validation of them was attempted in velocity or water surface elevation, but not in separation zones or stagnation zones, etc.

Therefore, the main objective of this study is to conduct a three-dimensional investigation of the effects of discharge ratios and junction angles on flows

characteristics associated with the primary and secondary flow patterns, shapes of separation zones, water depth, bed shear stress, kinetic energy, etc. at various confluences using appropriate numerical methodologies and validate the numerical results against the experimental results in order to implicate the result to other study fields such as bed morphology, sediment transport, ecology and so forth. Firstly, a grid independence study was conducted to find the optimal grid size for the simulation to save the computational time. Secondly, numerical investigations against discharge ratios based on the Shumate's experiment were carried out with the obtained optimal mesh and they were qualitatively validated by the point data of the experimental data. Thirdly, the other numerical investigation with various discharge ratios and junction angles based on Gurram et al.'s experiment was carried out and quantitative validations were conducted with the experimental data. Lastly, mathematical models were developed by Multiple Linear Regression to provide the simple estimation method of the flow characteristics and the sensitivity analysis using the sum of the partial derivatives was conducted to investigate the sensitivity of the discharge ratios and junction angles to the flow characteristics.

Chapter 2. Theoretical Background

2.1 Literature Review of Confluence flows

There have been several experiments about confluence flows in rectangular open channels to investigate the flow patterns of them. Firstly, Taylor (1944) was known as the first researcher who derived the mathematical models of confluence flows and conducted experiments of them at the rectangular channel with 45 and 135 degrees about the head losses around the junction zone. He mentioned that the size of the separation zone depends on the depth ratio between the branch and the main channel (Taylor, 1994). Then, Anwar (1955) carried out experiments with trapezoidal channels of different junction angles and widths and he found out that separation starts at the junction point on the main channel wall. Webber and Greated (1966) developed Taylor's study (1944) with some new techniques and additional junction angles with 30, 60, and 90 degrees since the results of them did not show a great agreement between theoretical results and experiment result. They expressed the energy loss and depth ratio between the upstream and downstream theoretically and experimentally. Lin and Soong (1979) conducted experiments with a 90-degree junction to investigate the boundary friction loss and the turbulent mixing loss. Best and Reid (1984) started to focus on shapes of separation zones at junctions, so they conducted some junction flow experiments with 15, 45, 70, and 90 degrees, different discharge ratios, and Froude numbers. The maximum widths and lengths of the separation zones for each case were measured and plotted to

find the relationship between them. It was found that the width and length of the separation zone increase with junction angle and discharge ratio (Best and Reid, 1984). Ramamurthy et al (1988) used the different momentums equation to the lateral and main channel separately and the application brought great accordance with their experimental result with 90-degree junction in terms of the depth ratios. Gurram et al (1997) conducted more and detailed experiments with 30, 60, 90 degrees, different discharge ratios, and Froude numbers. They plotted the relationship of them in terms of the pressure coefficient, depth ratio, the shape of the separation zone, lateral flow characteristic, and backwater effect. Hsu et al. (1998) conducted other junction experiments with 30, 45, 60, and 90 degrees, and different discharge ratios to find out the shape index of the separation zone, energy and momentum correction coefficients, flow angle, and depth and contraction coefficients. The described experiments measured velocities or water depths at only a few points or sections only with few two-component measurements. However, Shumate (1998) and Weber et al. (2001) conducted a remarkable and qualitative 90-degree junction experiment with different discharge ratios employing a three-component acoustic Doppler velocimeter (ADV). Velocity field contours and vector fields were firstly drawn in three components. Furthermore, water surface contours and turbulent kinetic energy were firstly plotted as well. However, the shape of the separation zone was not measured or calculated. Since the significant experiment was revealed, a large number of experiments about confluence flows have conducted with different junction angles, discharge ratios, Froude numbers, widths, and width

ratios (Choi et al., 2003 & 2004; Choi and Kim, 2006; Choi et al., 2006; Kwak and Rhee, 2012; Lee, 2013; Beharnagi et al., 2005; Qing-Yuan et al., 2007; Wang et al., 2007; Biswal et al., 2010; Mignot et al., 2012; Birjukova et al., 2012; Yoshimura et al., 2015; Coelho, 2015; Biswal et al., 2016; Creelle et al., 2016; Schindfessel, 2016; Yuan et al., 2016; Penna et al.,2018).

As results with better quality can be obtained with sophisticated instruments, numerical studies have initiated and attempted to validate their results with the experimental results while numerical methodologies have been improved significantly. Firstly, Bradbrook et al. (2001) attempted to validate Biron et al.'s experiment with discordance beds (1996). They adopted the SIMPLE (Semi-Implicit Method for Pressure Linked Equations) algorithm for velocity-pressure coupling and RNG k-ε turbulence closure model. It was found that junction angle and the magnitude of secondary circulation strength had a positive relationship and the discordance bed reduced water surface depression, pressure gradients but it caused stronger secondary circulation (Bradbrook et al., 2001). However, it was only validated against the 30 degrees results in velocity.

In addition, since the experiments of Shumate (1998) have published, their results were attempted to be validated against many numerical types of research. Huang et al. (2002) carried out the three-dimensional (3D) numerical study for 0.25 and 0.75 discharge ratio cases with 90-degree junction as the Shumate's experiment and an additional study with 30, 45, and 60 degrees. They selected

k-w turbulence model and PISO (Pressure-Implicit with Splitting of Operators) velocity-pressure coupling Algorithm. The results were visualized into water surface mapping, elevation profiles, velocity and vector fields, and streamlines. The result of the 90-degree case showed a good agreement, but the velocity profiles near the separation zone had some discordance near the wall. After Huang et al.'s numerical study and validation with Shumate's (1998), some numerical studies have been completed with Shumate's experiment (1998). Sivarkumar (2004) has conducted a 3D numerical study for only one case of Shumate's and attempted to validate the experiment in water depth in the x-axis with some discordance.

There were several trials to overcome the discordance with Shumate's experiment (1998) and improve numerical results with new mesh techniques or different turbulence models. Yang et al. (2013) employed a dynamic mesh technique that the grids change dynamically while the geometry changes with time as the water surface. Thus, it takes less time than Volume of Fraction (VOF) method. They conducted a 3D numerical study with k-ε, Realizable k-ε, k-ω turbulence models and dynamic mesh, rigid lid, VOF techniques and compare their results with the experimental results. It was realized that k-ε model showed the least accuracy and the k-ω model with dynamic mesh is a preferable model for confluence flows. Sharifipour (2015) conducted another 3-D numerical study with RNG k-ε, k-ε, and k-ω turbulence models and VOF method and compared the results of them and recognized that RNG k-ε and k-ω models showed much better agreement than k-ε model, but k-ω model was chosen as

the turbulence model for their study because it consumed less time than RNG k-ε model. The results were validated, but the vertical velocity profiles did not show good agreement near the bottom since the grid sizes near the wall were not fine enough. Additionally, a numerical study with different width ratios was carried out and it was found out that the size of the separation zone decreased as the width ratio increased.

Some numerical studies with different single-angle experiments were conducted and validated. Bonakdari et al.'s numerical study at a 30-degree junction (2011) with RSM model was tried to be validated against Wang et al.'s experiment (2007) and they reinforced the relationship between the separation zone shape and discharge ratios. Mignot et al. (2012) and Yoshimura et al. (2015) conducted a 90-degree experimental and numerical study with RNG k-e model and LES respectively together and validated their results.

Furthermore, some researchers attempted numerical studies with different angles to investigate the effect of them on the confluence flow. Bradbrook et al. (2001) as mentioned before and Biron et al. (2004) carried out a 3D numerical study of three different angles with RNG k-e model and validated the results against Biron et al (1996), but only for the 30-degree case due to the lack of experiments. Brito et al. (2014) carried out a 70-degree numerical study with a high width-depth ratio and validated it against Birjukova et al (2014). Penna et al. (2018) conducted a 70-degree experiment and numerical study of 45 to 90 degrees with k-e model. The branch channel width was much smaller than the

main channel. The numerical result could be validated only against a 70-degree experiment, but the results with different angles confirmed the fact that a higher junction angle causes larger retardation zones and separation zones. Shakibainia et al. (2010) conducted the same study at 15, 45, 90, 105 degrees with RNG k-e model and SIMPLE algorithm. The result was validated only against the Shumate's (1998) in velocity and water depth. Moreover, the maximum thickness of the separation zone was attempted to be validated against Hsu et al.'s experiment (1998) only for the 90-degree case with different discharge ratios. Choi et al. (2004) investigate the flow characteristics experimentally and numerically in the river open channel based on the real rivers in South Korea, but the numerical study was conducted with a 2D model.

The mentioned numerical studies above were attempted to be validated only against a single junction angle, but there were some numerical studies with comprehensive and quantitative validation with multiple-angle experiments. Ghostine et al. (2012) compared the 1D dynamic model and 2D Shallow water equations at the junctions and validated against Hsu et al. (1998), Hager (1989), Rice (1985), Christodoulou (1993) in terms of depth ratios. Luo et al. (2018) conducted a 3D numerical study for several junction angles and discharge ratios using SST k-w turbulence model, PISO algorithm, and finer meshes near the walls. The results were validated against Shumate's in a variety of aspects, and the 3D numerical results were compared with 1D analytic or empirical models from Shumate (1998), Hager (1989), Best & Reid (1984), Gurram et al. (1997), Hsu et al. (1998) and they showed reasonable agreement. However, only results

for 0.25 and 0.75 discharge ratios were presented graphically and only contraction coefficients related to the maximum width of separation zone was validated against the Gurram et al.'s experiment (1997), even there were more quantitative and absolute characteristic results in their experiment and more flow characteristic at the confluence to be investigated such as the secondary flow, depth depression, flow acceleration et cetera. Therefore, the 3D numerical simulation was conducted by employing some advanced methodologies or techniques found above in order to generate better results and validate the results in more aspects. The summaries of the studies are described in Table 1 and Table 2.

Table 1. Summary of previous studies about open-channel experimental studies

Author	Year	Angle (degree)	q*	Fr	W (m)	W/h	Type
Taylor	1944	45, 135	0.2, 0.4, 0.6	0.20-0.75	0.102	n/a	Experiment
Anwar	1955	22.5, 45, 67.5, 90	0.5, 0.67, 1	0.47-0.53	0.584-0.690	4.95-5.43	Experiment
Webber and Greated	1966	30, 60, 90	0, 0.2 0.4, 0.5, 0.6, 0.8, 1	0.20-0.60	0.127	n/a	Experiment
Lin and Soong	1979	90	0.54-0.85	0.65-1.15	0.457	4.88-7.14	Experiment
Best and Reid	1984	15, 45, 70, 90	0.1-0.9	0.10-0.30	0.15	n/a	Experiment
Ramamurthy et al	1988	90	0.32-0.88	0.20-0.80	0.248	2.86	Experiment
Biron et al.	1996	30	0.448	0.2	0.15	0.94	Experiment
Gurram et al	1997	30, 60, 90	0, 0.25, 0.5, 0.75, 1	0.25-1.00	0.5	5.00-8.33	Experiment
Hsu et al.	1998	90	0.1-0.9	0.45-0.53	0.155	1.7-2.6	Experiment
Hsu et al.	1998	30, 45, 60	0.08-0.91	0.45-0.62	0.155	1.70-2.38	Experiment
Webber et al.	1998	90	0.08-0.92	0.37	0.914	3.09	Experiment
Choi et al.	2003	30, 45, 60, 75, 90	0.2, 0.5, 0.375, 0.8	0.2-0.5	0.32,0.4	5.33, 10	Experiment
Choi et al.	2003	90	0.2, 0.5, 0.375, 0.8	0.22	0.32, 0.4	1.6, 2	Experiment
Choi et al.	2003	30, 45, 60, 75, 90	0.2, 0.5, 0.375, 0.8	0.07, 0.10, 0.14	0.32, 0.4	5.33, 10	Experiment
Beharnagi et al.	2005	45, 90	0.05-0.95	0.22-0.53	0.4	1.34-2.41	Experiment
Choi et al.	2006	30, 45, 60, 75, 90	0.17, 0.33, 0.44	0.384-0.438	0.32, 0.4	0.8, 1	Experiment
Wang et al.	2007	30	0.43	0.5	0.4, 1	2.86, 7.14	Experiment
Yang et al.	2009	90	0.74	0.2	1	3.64	Experiment
Biswal et al.	2010	90	0.32-0.68	0.04	0.82	3.71	Experiment
Kwak and Rhee	2012	60, 75	0.25, 0.4, 0.5	0.5-1.5	0.5, 0.75, 0.1	1.25-2.5	Experiment
Lee	2013	30, 60, 90	0.09, 0.105, 0.125, 0.154, 0.2	0.044-0.091	0.3, 1	0.6, 0.1	Experiment
Birjukova et al.	2014	70	0.9	0.49	1	10	Experiment
Pinto Coelho	2015	30, 60	0.25-0.74	0.60-0.70	0.3	2.36-4.92	Experiment
Creelle et al.	2016	90	0.08-0.92	0.37	0.4	3.09	Experiment
Yuan et al.	2016	90	0.4	0.08	0.4	2.5	Experiment
Biswal et al.	2016	90	0.25-0.75	0.09	0.2	0.91	Experiment

Table 2. Summary of previous studies about open-channel numerical or experimental studies

Author	Year	Angle (degree)	q*	Fr	W (m)	W/h	Width ratio	Type	Dimension	Turbulence model
Choi and Kang	1993	30, 60, 90	0.4	0.2, 0.4, 0.6	-	-	-	Numerical	1D	Moment equation
Bradbrook et al.	2001	30, 45, 60	0.448	0.2	0.15	0.94	0.4	Numerical	3D	RNG-ke
Huang et al.	2002	90	0.25, 0.75	0.37	0.914	3.09	1	Numerical	3D	k-w
Sivakumar et al.	2004	90	0.25	0.37	0.914	3.09	1	Numerical	3D	-
Biron et al.	2004	30, 60, 90	0.448	0.2	0.15	0.94	0.4	Numerical	3D	RNG-ke
Cho et al.	2005	90	0.16, 0.33, 0.44	0.07, 0.10, 0.14	0.32, 0.4	5.33, 10	0.46	Numerical	2D	RMA2
Ahn et al.	2006	30, 60, 90	0.17, 0.29, 0.38	-	0.25, 0.5, 1	-	0.17, 0.33, 0.67	Numerical	2D	RMA2
Cho	2007	30, 60, 90	0.091, 0.167, 0.250	0.55	0.3	1.74-9.43	0.2	Numerical	1D	FLDWAV
Shakibainia et al.	2010	15, 45, 90, 105	0.25, 0.5, 0.75	0.26, 0.34, 0.43	0.914	-	0.66, 1	Numerical	3D	RNG-ke
Bonakdari et al.	2011	30	0.43	0.5	0.4, 1	2.86, 7.14	0.4	Numerical	3D	RSM
Song	2011	90	0.25	0.37	1	3.09	1	Numerical	2D	Unsteady 2D depth-averaged model
Ghostine et al.	2012	30-90	0-1	-				Numerical	1D, 2D	1D Sainet-Venant equation, 2D shallow water equation
Mignot et al.	2012	90	0.25, 0.75	0.1	0.3	2.5		Experiment & Simulation	3D	RNG k-e
Djordjevic	2013	90	0.77	0.37	0.914	3.09	1	Numerical	3D	k-e
Yang et al.	2013	90	0.25	0.37	0.914	3.09	1	Numerical	3D	k-e, Realizable k-e, k-w, k-w (Rigid-lid surface), k-w (VOF)
Brito et al.	2014	70	0.9	0.49	1	10	-	Numerical	3D	-
Yoshimura et al.	2015	90	0.5, 0.8	0.48, 0.30	0.5	10		Experiment & Simulation	3D	LES
Sharifipour	2015	90	0.25, 0.75	0.37	0.914	3.09	0.5-2	Numerical	3D	RNG k-e, k-e and k-ω (at the end)

Table 2. Summary of previous studies about open-channel numerical or experimental studies -Continued

Schindfessel et al.	2015	90	-	-	0.98	2.36	1	Experiment & Simulation	3D	LES
Schindfessel et al.	2016	90	0.05, 0.25	0.05	0.98	2.36	1	Experiment & Simulation	3D	LES
Luo et al.	2018	90; 30,45,60,90	0.25, 0.75; 0.083-0.917	0.37	0.914	3.09	1	Numerical	1D, 3D	k-w SST
Penna et al.	2018	70(exp),45-90(Num)	0.11	-	0.15, 1	9.09, 1.36	1	Experiment & Simulation	3D	k-e
Ramos et al.	2019	90	0.25	0.37	0.914	3.09	1	Numerical	3D	LES

2.2 Flow Characteristic in Junction Channels

The confluence flow around a junction shows various flow characteristics as Figure 1, 2, and 3. Firstly, the flow stagnation zone exists at the upstream junction corner due to the flow detachment at the junction. Secondly, the flow from the branch channel is deflected when it meets the main flow, and it is called the flow deflection zone. Thirdly, the flow separation zone or recirculation zone is formed from the downstream corner and the flow recirculates in the zone due to the momentum from the branch flow detaching the flow at the downstream corner of the junction, and the flow is recirculated in the zone. Fourthly, water level depression occurs in the vicinity of the downstream junction corner due to the backwater characteristics caused by energy loss. Fifthly, the water level also increases around the combining area and it is called, water level afflux zone due to the same reason above. Sixthly, the streamline from the stagnation point and that of the separation zone are called shear layers. Seventhly, the shear layers contract the flow and they increase the velocity of the flow and maximum velocity zone or flow contraction zone is generated. Eighthly, flow recovery zone is where the flows are mostly fully combined, the backwater effect is diminished, and a uniform flow is dominant. Lastly, the helicoidal secondary flows due to an orientation change can be observed as shown in Figure 3. When the discharge ratio is low, two secondary flows can be found around the separation zone developed by the shear layer and mixing layer. However, when the discharge ratio is high, the secondary flow by the mixing layer is conflicted to the right wall and diminishes

before the separation zone since the lateral flow pushes the main flow. The conflicted flow can be impinged back and generate another helical flow. Moreover, the 3-dimensional view showed that the flow characteristics should be illustrated and simulated in three dimensions as presented in Figure 4. The separation zone gets smaller while the depth gets deeper and the shear plane has helical shape-changing in the water depth.

Therefore, it is essential to conduct a numerical study of the confluence in three dimensions rather than 2 dimensions in order to accurately simulate the flow characteristics.

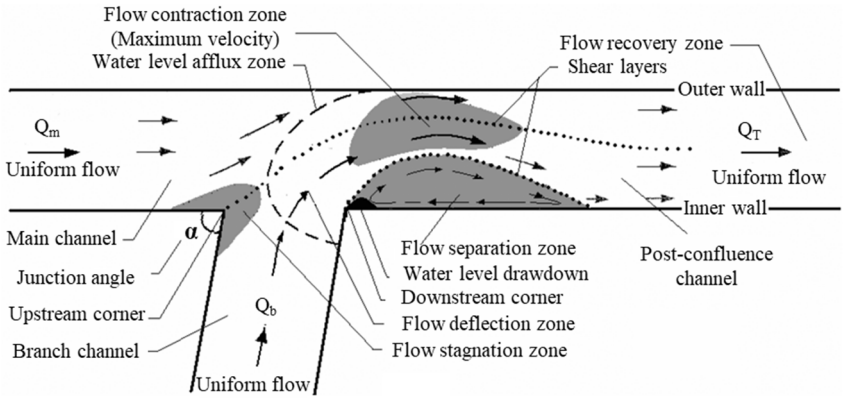

Figure 2. Plan view of flow characteristics for confluence flow in an open channel (Shakibainia et al., 2010)

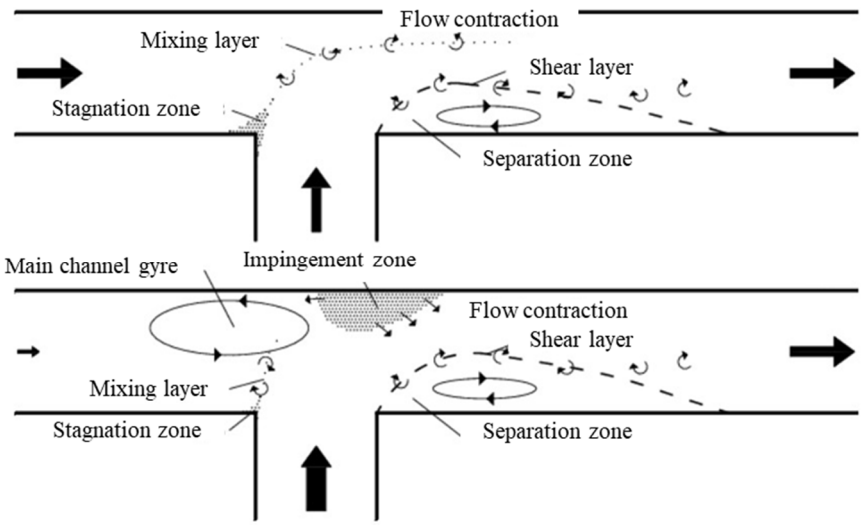

Figure 3. Secondary flow characteristics for confluence flow in an open channel for low q* (top) and high q* (bottom) (Schindfessel, 2016)

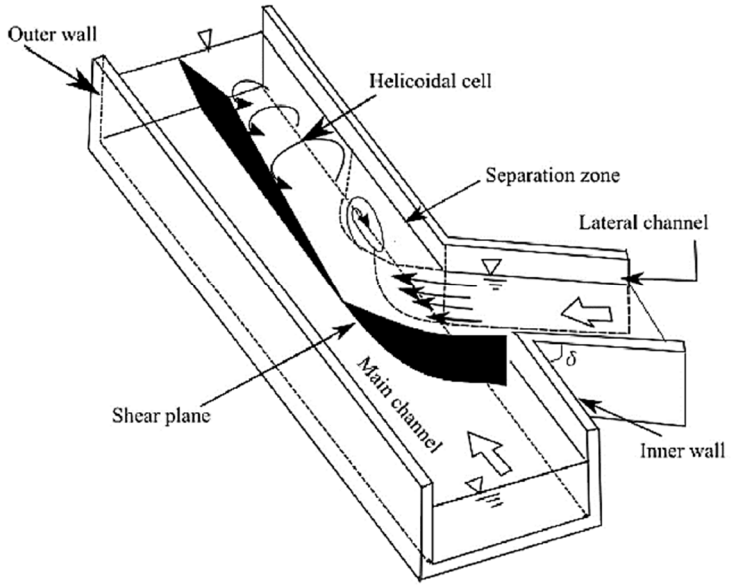

Figure 4. 3D view of flow characteristics for confluence flow in an open channel (Luo et al., 2018)

Chapter 3. Methodology

The entire numerical investigation was solved by OpenFOAM which an open-source software for CFD based on the Finite Volume Method (FVM) by utilizing parallel computing systems.

3.1 Governing Equations

The Reynolds-Averaged Navier-Stokes (RANS) equations with Boussinesq's approximation for incompressible flows was solved for this numerical study. The governing equations are expressed in the Cartesian tensor form below.

Continuity equations are expressed below

$$\frac{\partial \overline{u_i}}{\partial x_i} = 0 \tag{1}$$

Momentum equations are expressed below

$$\frac{\partial \overline{u_i}}{\partial t} + \overline{u_j}\frac{\partial \overline{u_i}}{\partial x_j} = \overline{f_i} - \frac{1}{\rho}\frac{\partial \overline{p}}{\partial x_i} + \nu\frac{\partial^2 \overline{u_i}}{\partial x_j \partial x_j} + \nu_t \frac{\partial^2}{\partial x_j}\left(\left(\frac{\partial \overline{u_i}}{\partial x_j} + \frac{\partial \overline{u_j}}{\partial x_i}\right) - \frac{2}{3}k\delta_{ij}\right) \tag{2}$$

$$k = \frac{1}{2}\overline{u'_i u'_i}$$

Where $\overline{u_i}$ is the mean velocity, $\overline{p}$ is the mean pressure, $\overline{f_i}$ is the external force, ν is the kinematic viscosity, ν_t is turbulence eddy viscosity, k is the turbulence kinetic energy, δ_{ij} is the Kronecker delta (δ_{ij}=0, if $i \neq j$, δ_{ij}=1, if $i = j$).

The turbulent eddy viscosity, v_t is unknown in the momentum equations, so it is necessary to be modeled. In this research, SST k-ω model (Menter, 1994) as a combined model between k- ε and k- ω model was employed since it predicts flow separation better than the standard k-ω model (Bardina, Huang, & Coakley, 1997) and it showed better validations than some models with chosen experiments as mentioned above (Yang et al., 2013 & Sharifipour, 2015).

The k and ω equations of the model describing turbulence kinetic energy and specific dissipation rate are expressed below.

k equation is illustrated below

$$\frac{\partial k}{\partial t} + \overline{u}_j \frac{\partial k}{\partial x_j} = P_k - \beta^* k\omega + \frac{\partial}{\partial x_j}\left[\left(\nu + \sigma_k \nu_t \right) \frac{\partial k}{\partial x_j} \right] \tag{3}$$

ω equation is illustrated below

$$\frac{\partial \omega}{\partial t} + \overline{u}_j \frac{\partial \omega}{\partial x_j} = \alpha S^2 - \beta \omega^2 + \frac{\partial}{\partial x_j}\left[\left(\nu + \sigma_\omega \nu_t \right) \frac{\partial \omega}{\partial x_j} \right] + 2(1 - F_1)\sigma_{\omega 2} \frac{1}{\omega} \frac{\partial k}{\partial x_i} \frac{\partial \omega}{\partial x_i} \tag{4}$$

The k and ω can be solved by the above equations, then the turbulence eddy viscosity, v_t can be calculated with the obtained k and ω values by the equations below (Menter et al., 2003). The standard k-ω model's ν_t value is simply k/ω, but the calculation of SST k-ω model is more complicated with a few coefficients which have been determined by several types of research for years.

Turbulence eddy viscosity, v_t and the coefficients are presented below

$$
\begin{gathered}
v_t = \frac{a_1 k}{\max\left(a_1\omega, SF_2\right)} \\
F_2 = \tanh\left[\left[\max\left(\frac{2\sqrt{k}}{\beta^*\omega y}, \frac{500v}{y^2\omega}\right)\right]^2\right] \\
P_k = \min\left(\tau_{ij}\frac{\partial \overline{u_i}}{\partial x_j}, 10\beta^* k\omega\right) \\
F_1 = \tanh\left\{\left\{\min\left[\max\left(\frac{2\sqrt{k}}{\beta^*\omega y}, \frac{500v}{y^2\omega}\right), \frac{4\sigma_{\omega 2}k}{CD_{k\omega}y^2}\right]\right\}^4\right\} \\
CD_{k\omega} = \max\left(2\rho\sigma_{\omega 2}\frac{1}{\omega}\frac{\partial k}{\partial x_i}\frac{\partial \omega}{\partial x_i}, 10^{-10}\right) \\
\phi = \phi_1 F_1 + \phi_2\left(1 - F_1\right) \\
\alpha_1 = \frac{5}{9}, \alpha_2 = 0.44 \\
\beta_1 = \frac{3}{40}, \beta_2 = 0.0828 \\
\beta^* = 0.09 \\
\sigma_{k1} = 0.85, \sigma_{k2} = 1 \\
\sigma_{\omega 1} = 0.5, \sigma_{\omega 2} = 0.856
\end{gathered}
\tag{5}
$$

Where S is the invariant measure of the strain rate, $\sqrt{2S_{ij}S_{ij}}$

3.2 Near Wall Model

Wall functions were employed to simulate the turbulence profiles near the wall since the grids are not fine enough to solve the boundary layer near the wall due to the computation time (Mentor et al., 2003). The turbulent kinetic energy, *k* is assumed to be a zero flux. The specific dissipation rate, *ω* in the linear and the logarithmic near-wall zone are described below (Mentor et al.,

2003)

$$\omega_{vis} = \frac{6\nu}{0.075 y^2}$$
$$\omega_{\log} = \frac{1}{0.3\kappa}\frac{u_\tau}{y} \tag{6}$$

Where ω_{vis} and ω_{log} are the specific dissipation rates for viscous and logarithmic layers respectively, and κ is the Von-Karman constant.

The intermediate region can be calculated as presented below,

$$\omega = \sqrt{\omega_{vis}^2 + \omega_{\log}^2} \tag{7}$$

The friction velocity profile near the wall was solved by the equation below

$$u_\tau^{vis} = \frac{U}{y^+}$$
$$u_\tau^{\log} = \frac{U}{\frac{1}{\kappa}\ln(y^+) + C} \tag{8}$$

Where u_τ is the friction velocity on the wall, U is the mean velocity, y^+ is the non-dimensional y.

The velocity profile in an intermediate region can be expressed as the specific dissipation rate above,

$$u_\tau = \sqrt[4]{\left(u_\tau^{vis}\right)^4 + \left(u_\tau^{\log}\right)^4} \tag{9}$$

The turbulent viscosity can be modeled as expressed below (Liu, 2016),

$$v_t = v \cdot \left(\frac{ky^+}{\ln\left(Ey^+\right)} - 1 \right) \tag{10}$$

Where E is the wall smoothness coefficient which is 9.8 for the smooth walls.

3.3 Computational Domain

The domains of water and air of the channel as the experiment of Shumate (1998) and Gurram et al. (1997) were generated with the multi-block algorithm which divides the domains into several parts with optimal grid sizes and the downstream parts of each experiment were clipped to reduce the computational time. The created domains for each case were meshed with the structured method by Gmsh software. The areas around the confluence where significant variations of flows occur were meshed finer than the others and the walls were meshed finer to simulate the boundary layer properly.

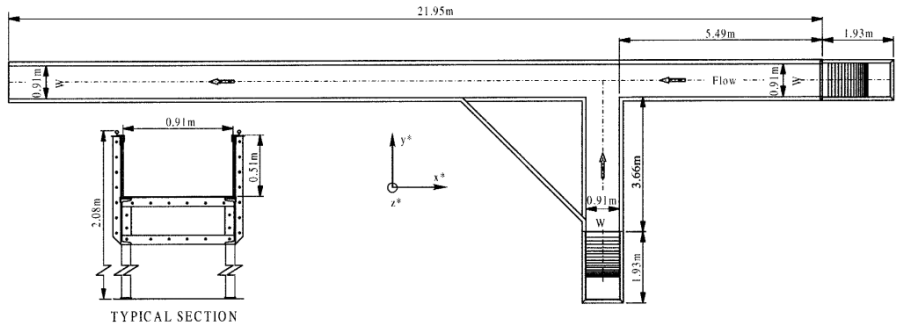

Figure 5. Experimental layout of the experiment by Shumate (1998)

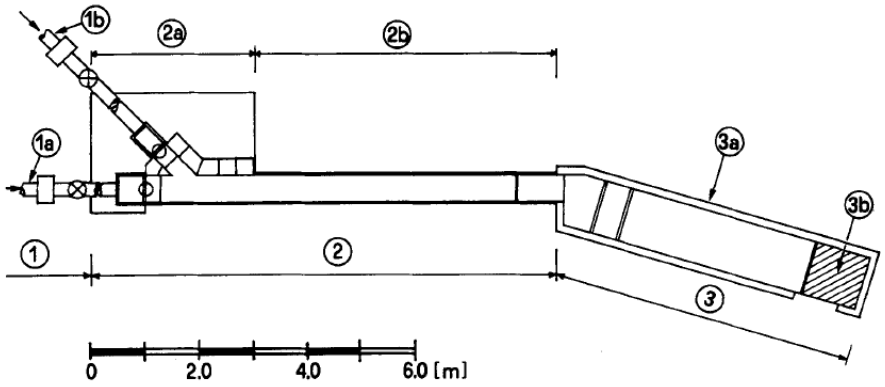

Figure 6. Experimental layout of the experiment by Gurram et al. (1997)

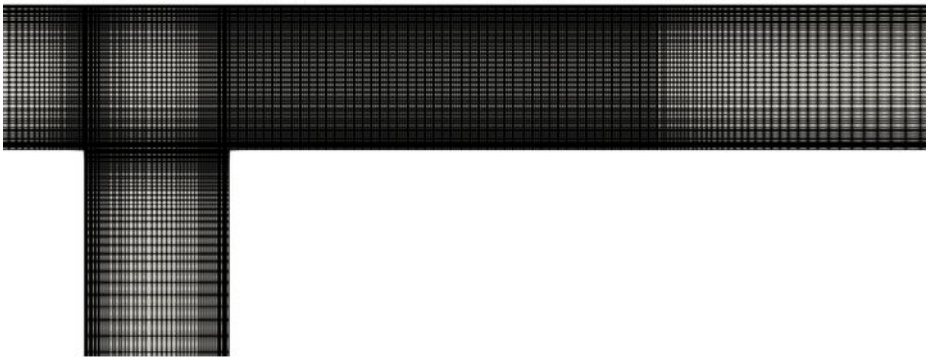

Figure 7. Simulation grid near a junction of the experiment by Shumate (1998)

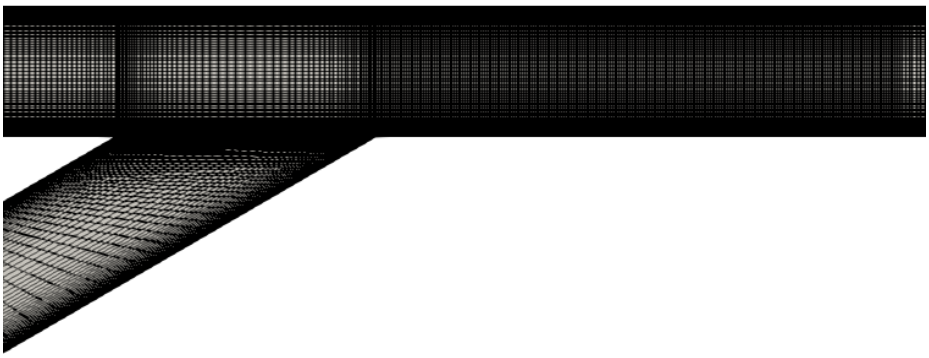

Figure 8. Simulation grid near a junction of the experiment by Gurram et al. for 30 degrees (1997)

3.4 Discretization Numerical Schemes

OpenFOAM is based on the Finite Volume Method (FVM) and the discretization Schemes for each term are listed in Table 3 below.

Table 3. FVM discretization schemes

Type	Method
Time derivative	Euler
Gradient	Gauss linear
Divergence	Gauss linear
Laplacian	Gauss linear corrected
Interpolation	Linear
Gradient normal	Corrected

3.5 Free Surface Treatment

Volume of Fluid (VOF) method was used to model the free surface for this study. It can model an interface between two or more different fluids by tracking the volume fraction of the fluids while solving the momentum equations in the computational domain. The interphase between the two fluids was solved by the equation below.

$$\frac{\partial \alpha}{\partial t} + \frac{\partial \left(\alpha u_j \right)}{\partial x_j} = 0 \tag{11}$$

Where α is 1 for water, and α is 0 for air.

3.6 Boundary and Initial Conditions

The boundary condition was set to be the same as each experimental condition. The general boundary condition for each case is listed in Table 4 and Table 5.

Table 4. General boundary condition of simulations part 1 of 2

alpha.water		
	Type	Value
walls	zeroGradient	-
Outlet of water	zeroGradient	-
Outlet of air	zeroGradient	-
Inlet of water	uniform	1
Inlet of air	uniform	0
interphase	inletOutlet	0
k		
	Type	Value
walls	kqRWallFunction	Variable
Outlet of water	zeroGradient	-
Outlet of air	zeroGradient	-
Inlet of water	fixedValue	Variable
Inlet of air	fixedValue	Variable
interphase	inletOutlet	Variable
w		
	Type	Value
walls	omegaWallFunction	Variable
Outlet of water	zeroGradient	-
Outlet of air	zeroGradient	-
Inlet of water	fixedValue	Variable
Inlet of air	fixedValue	Variable
interphase	inletOutlet	Variable

Table 5. General boundary condition of simulations part 2 of 2

nut		
	Type	Value
walls	omegaWallFunction	0
Outlet of water	zeroGradient	-
Outlet of air	zeroGradient	-
Inlet of water	calculated	0
Inlet of air	calculated	0
interphase	calculated	0
p_rgh		
	Type	Value
walls	zeroGradient	
Outlet of water	fixedFluxPressure	0
Outlet of air	zeroGradient	-
Inlet of water	zeroGradient	-
Inlet of air	zeroGradient	-
interphase	totalPressure	0
U		
	Type	Value
walls	noSlip	-
Outlet of water	flowRateOutletVelocity	Variable
Outlet of air	zeroGradient	-
Inlet of water	flowRateInletVelocity	Variable
Inlet of air	fixedValue	0
interphase	pressureInletOutletVelocity	0

The initial values of the kinematic viscosity and specific dissipation rate were calculated by the equations below.

$$k = \frac{3}{2}(UI)^2$$
$$\omega = \frac{k^{0.5}}{C_\mu L} \quad (12)$$

Where I is a turbulence intensity assumed to be 5%, C_μ is a constant equal to 0.09, L is a reference length which is half of the channel width.

For the Shumate's case, the junction angle is 90 degrees and the water depths of both inlets are 0.33m and the Froude number is around 0.37 and the conditions of volumetric flow rates of main and branch inlet, Q_m and Q_b, is listed in Table 6. The q^* is the ratio of the branch channel flow rate to the downstream flow rate.

Table 6. Flowrate condition of the simulation of Shumate (1998)

Q_b (m^3/s)	Q_m (m^3/s)	q*
0.042	0.127	0.25
0.127	0.042	0.75

For Gurram et al.'s case, the junction angles are 30, 60, and 90 degrees, and the water depths of both inlets are 0.1m. The Froude number is 0.5 and the flowrate conditions are listed in Table 7

Table 7. Flowrate condition of the simulation of Gurram et al. (1997)

Q_b (m^3/s)	Q_m (m^3/s)	q^*
0.0062	0.0187	0.25
0.0124	0.0124	0.5
0.0187	0.0062	0.75

3.7 Velocity-Pressure Coupling Algorithm

PIMPLE (Pressure Implicit Method for Pressure-Linked Equations) algorithm was used to couple between velocity and pressure in order to solve Navier-Stokes equations. It is a combined algorithm between PISO (Pressure Implicit with Splitting of Operator) and SIMPLE (Semi-Implicit Method for Pressure-Linked Equations). PISO is a non-iterative computation algorithm for complicated transient flow calculation with large time steps while SIMPLE is an iterative algorithm for not complicated flow. PIMPLE algorithm is an iterative PISO algorithm, so it is more stable and accurate than the other two methods (The OpenFoam Foundation, 2019). The flow chart of the PIMPLE is illustrated in Figure 9.

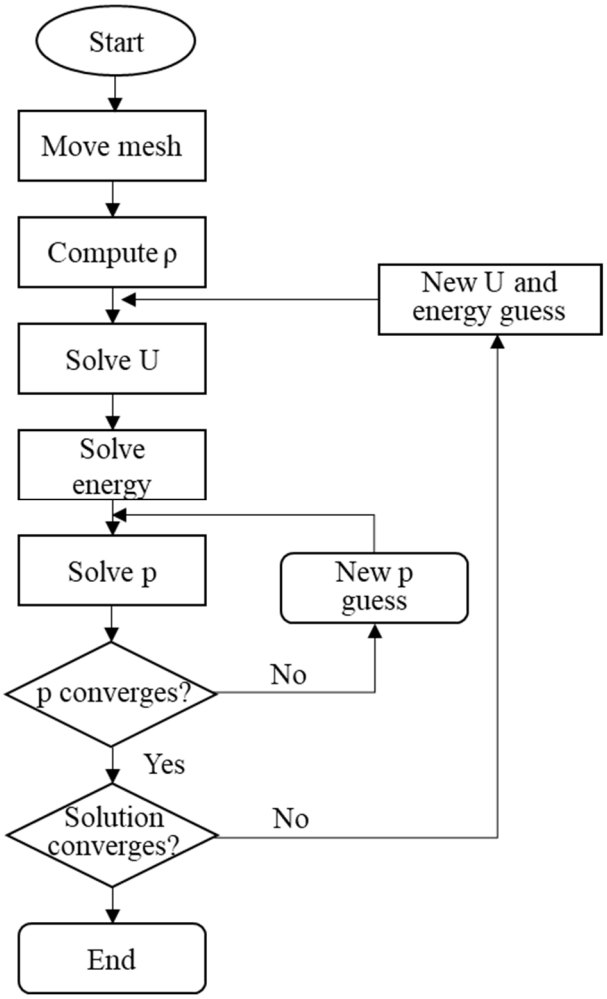

Figure 9. Flow chart of PIMPLE algorithm (Garcia-Alcaide et al, 2017)

3.8 Multiple Linear Regression and Sensitivity Analysis

Multiple linear regression (MLR) was employed to develop simple models to estimate the flow characteristics including the width and length of the separation zone, maximum u velocity, maximum bottom shear stress, minimum depth ratio. The general MLR equation is presented below. The coefficients of them were estimated by the least-squares method which is to minimize the sum of the squares of the residuals fitting the variables in linear lines.

$$y_i = \beta_0 + \beta_1 x_{i1} + \beta_2 x_{i2} + \ldots + \beta_p x_{ip} + e \tag{13}$$

Where y_i are dependent variables, x_i are explanatory variables β_0 is the y-intercept, β_p are slope coefficients for each explanatory variable and e is the error term.

Furthermore, adjusted R-squared was used to judge the goodness-to-fit of the calculated coefficients rather than R-squared since the explanatory variables are more than one. It can be said that the model is a more accurate model to estimate the values if the R-squared is closer to 1.

$$Adjusted\ R^2 = 1 - \frac{SS_{residuals} / (n - K)}{SS_{total} / (n - 1)} \tag{14}$$

Where $SS_{residuals}$ is the residual sum of squares, SS_{total}, is the total sum of squares, n is the number of data points, and K is the number of parameters.

Moreover, the Mean Squared Error (MSE) was employed as an estimator.

$$MSE = \frac{1}{n}\sum_{i=1}^{n}\left(Y_i - \widehat{Y}_i\right)^2 \tag{15}$$

Where Y_i is the observed value, and $\widehat{Y}_i$, is the predicted value.

The Mean of the Partial Derivates (MPD) was computed to see the sensitivity of the flow characteristics to the discharge ratio and the junction angle. The high MPD means the high sensitivity to x_i

$$MPD = \frac{1}{n}\sum\left|\frac{\Delta y_i}{\Delta x_i}\right| \tag{16}$$

Where y_i is the flow characteristic and x_i is the discharge ratio, q* or junction angle ratio, angle* (angle/90°).

Chapter 4. Results and Validation

A numerical study was conducted by the mentioned methodology and validated based on the experiment of Shumate (1998) and Gurram et al. (1997). The flow directions were reoriented for the consistent illustration. The q* is the discharge ratios between the branch and downstream discharge rates. x*, y*, and z* are the non-dimensional coordinates by the channel width.

4.1 Grid Independence Study

Firstly, the optimal number and size of grids were investigated by a grid independence study. Figure 10 demonstrates that the length of the separation zone of Shumate's when q* is 0.25 was converged while the number of cells increased, and the size decreased near the walls. This implies that the mesh with 2760000 cells was fine enough and the results would not change significantly with even finer mesh.

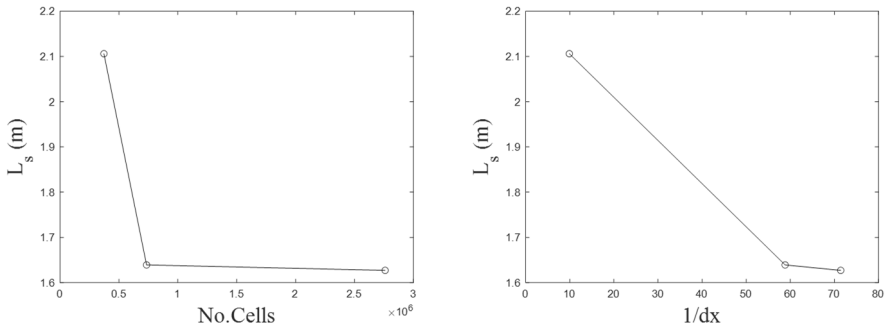

Figure 10. Grid independence study of the length of the separation zone

4.2 Discharge ratio study with the experiment of Shumate (1998)

The effect of the discharge ratio has been simulated and comprehensively validated against Shumate's experimental point data (1998). The discharge ratio was set to be 0.25 and 0.75 and the Froude number is determined to be around 0.37. The Reynolds number was $2.07*10^5$. However, the values near the wall could not be measured in the experiment, so the values near the wall were linearly interpolated.

Non-dimensional surface velocity fields by the downstream velocities of the experiment and simulation of u components for q*=0.25 and 0.75 were plotted as shown in Figure 11 and Figure 12. In general, the flow patterns were similar between experiment and numerical results, and the separation zones were considered to increase as the discharge ratio increased. However, it was difficult to measure and compare the size of the separation zone due to the small experimental data grids. Moreover, the magnitude and the size of the maximum velocity zones were observed above the separation zones and they increased as the discharge ratio increased because the separation zones increased. The simulation results tended to expect the maximum velocity zone larger and delayed being reattached.

The vectors of them were graphed in Figure 13 and Figure 14 and it was investigated the separation zone changes with different discharge ratios. The reattachment of the simulation went slower than the experiment as shown near the top wall as mentioned with the velocity fields.

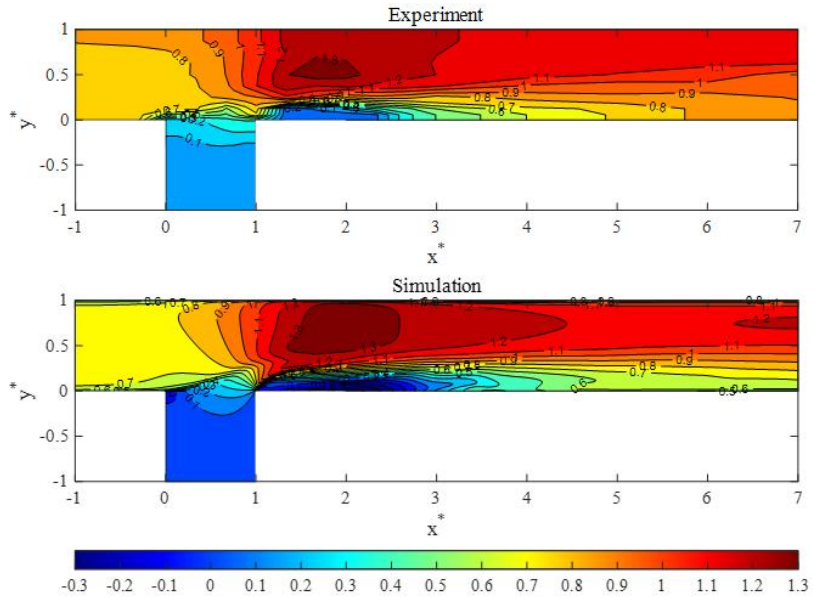

Figure 11. Non-dimensional surface u velocity fields for q^*=0.25

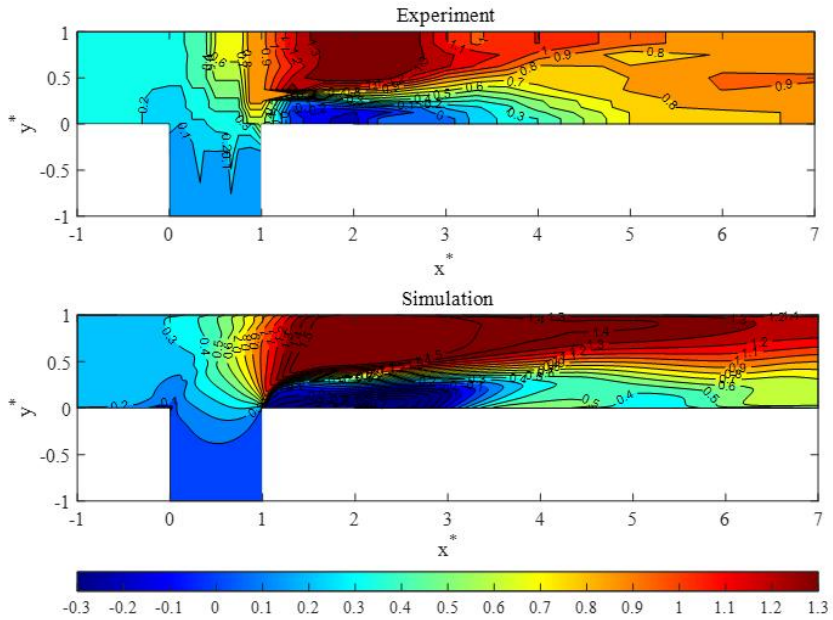

Figure 12. Non-dimensional surface u velocity fields for q^*=0.75

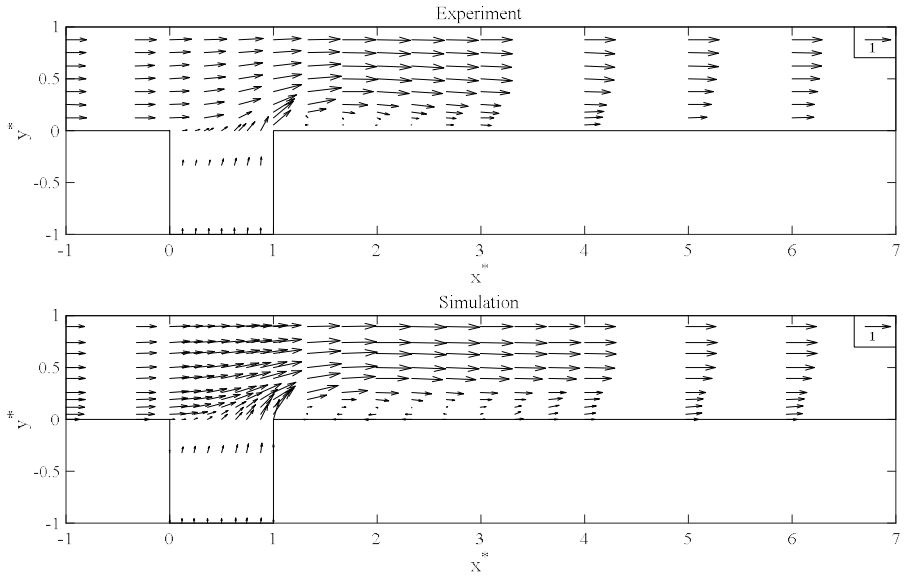

Figure 13. Surface vector fields for q^*=0.25

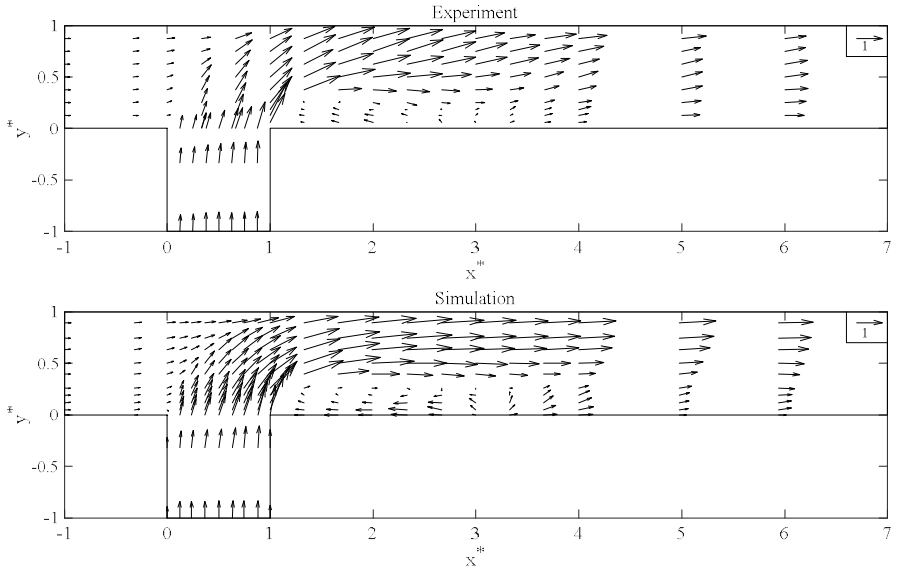

Figure 14. Surface vector fields for q^*=0.75

The velocity profiles for each discharge ratios were compared in the top view and cross-section view in Figure 15 and Figure 16. The top view u* profiles showed a reasonable agreement especially around the separation zones, but as the velocity contour fields demonstrated, the downstream velocities were discordant due to the late flow recovery of the simulation. Furthermore, the u* velocity profiles were illustrated in Figure 17 and Figure 18. They agreed reasonably with the experiments, especially near the walls but the profiles after separation zones had discordances due to the late flow recovery of the simulation. It was found that the velocity profiles varied more near the wall with high discharge ratios due to the larger velocity from the lateral flow.

v*-w* velocity vector field when x* = 5 for q*=0.25 and 0.75 were illustrated in Figure 19 and Figure 20 where it was behind the separation zone to scrutinize the effect of the discharge ratios to the secondary flow. It was discovered that one clockwise secondary flow was formed near the wall close to the branch and the other anticlockwise secondary flow was developed the opposite wall when the discharge ratio is 0.25. On the other hand, the flow of the 0.75 discharge ratio generated a single and bigger clockwise secondary flow in the entire section. More vector plots at the different x* were attached in Appendix A.

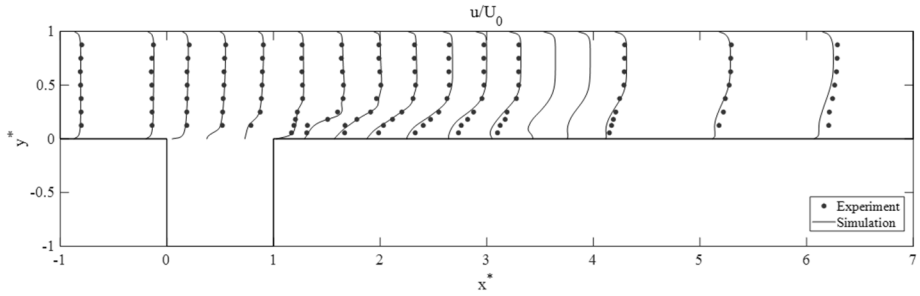

Figure 15. Top view of u* profile for q* = 0.25 and z* = 0.278

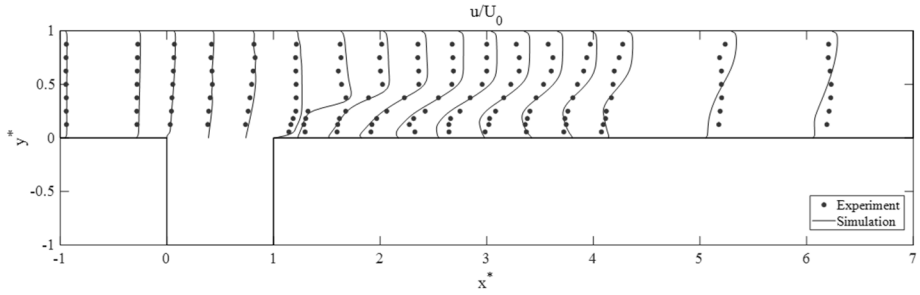

Figure 16. Top view of u* profile for q* = 0.75 and z* = 0.278

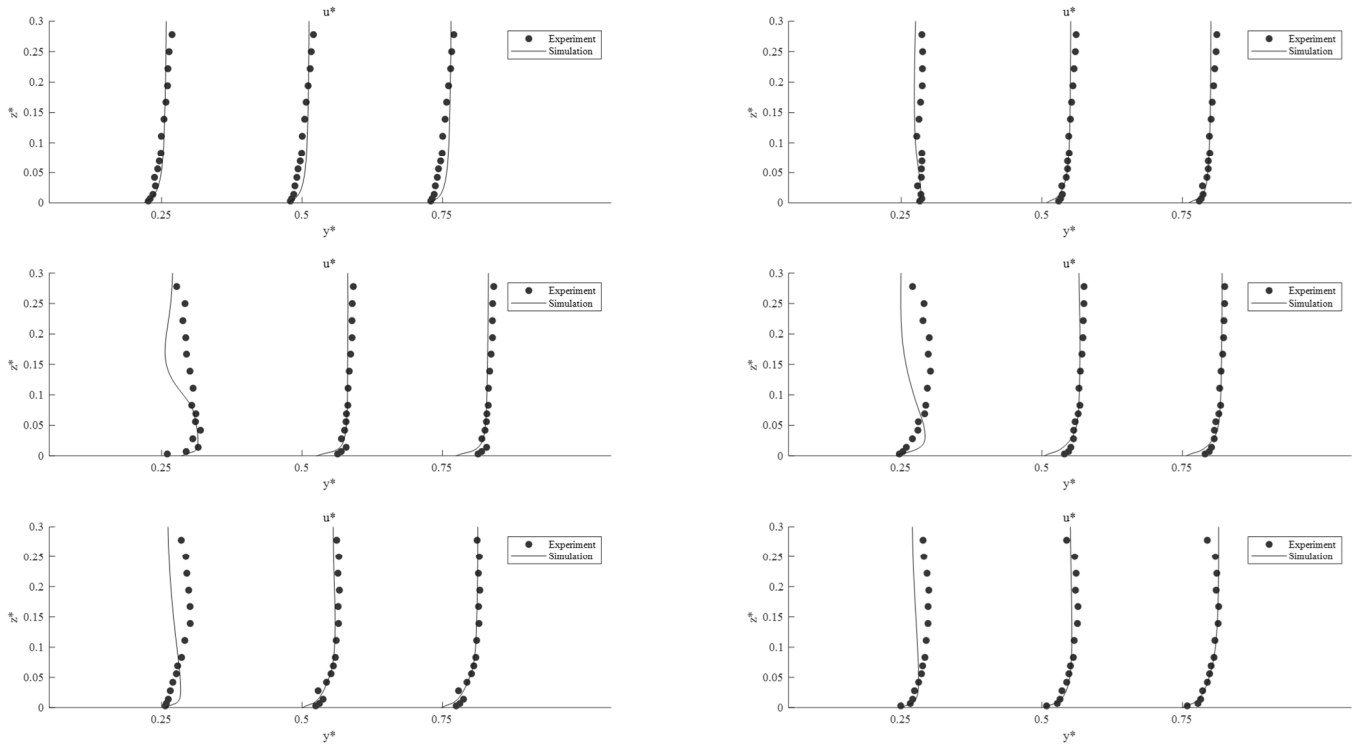

Figure 17. Velocity profiles of u* in cross-sections for q^*=0.25 and x*=0, 1, 2, 3, 5, and 7

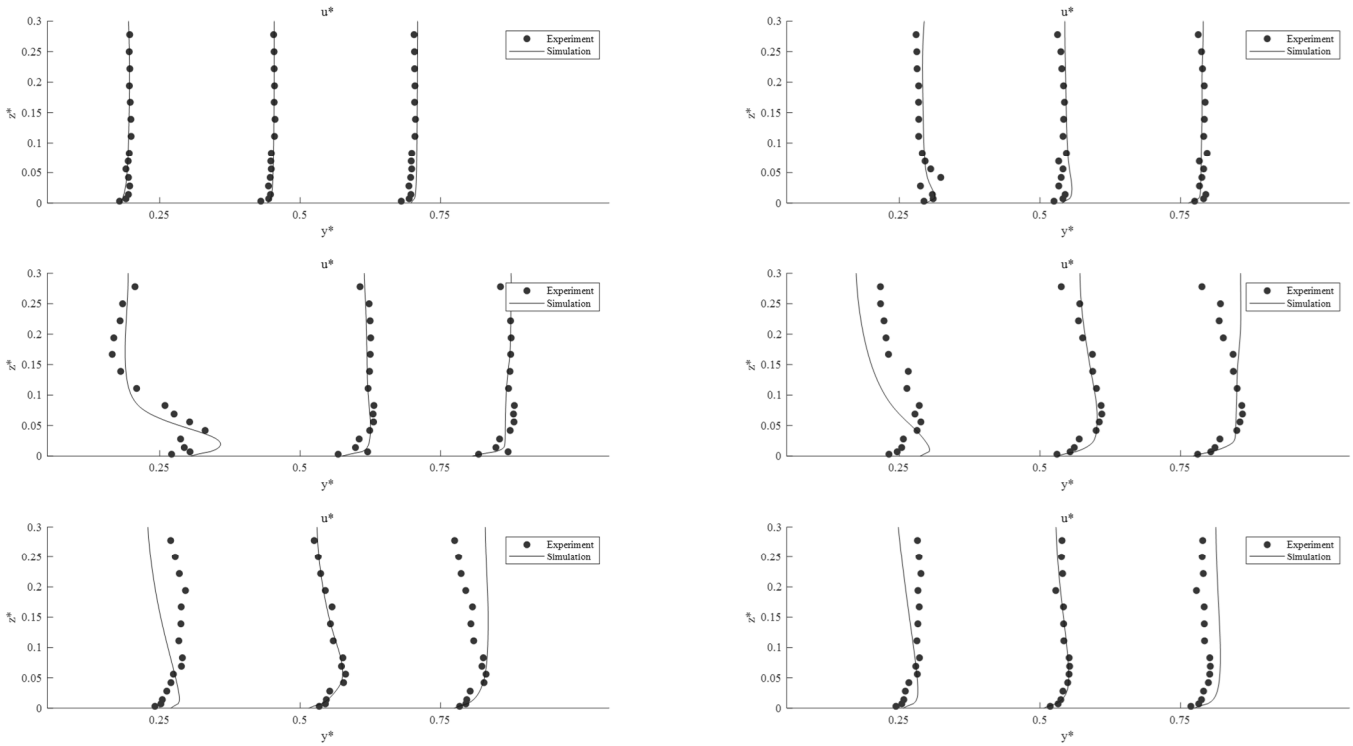

Figure 18. Velocity profiles of u* in cross-sections for q^*=0.75 and x*=0, 1, 2, 3, 5, and 7

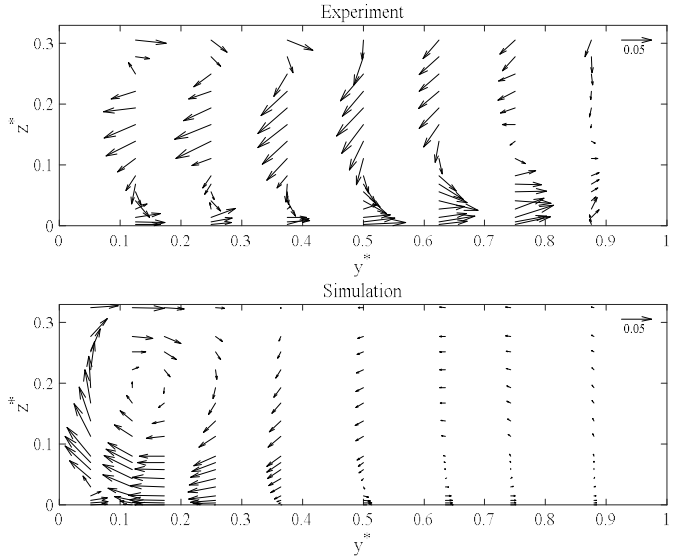

Figure 19. v*-w* velocity vector field for q*=0.25 and x* = 5

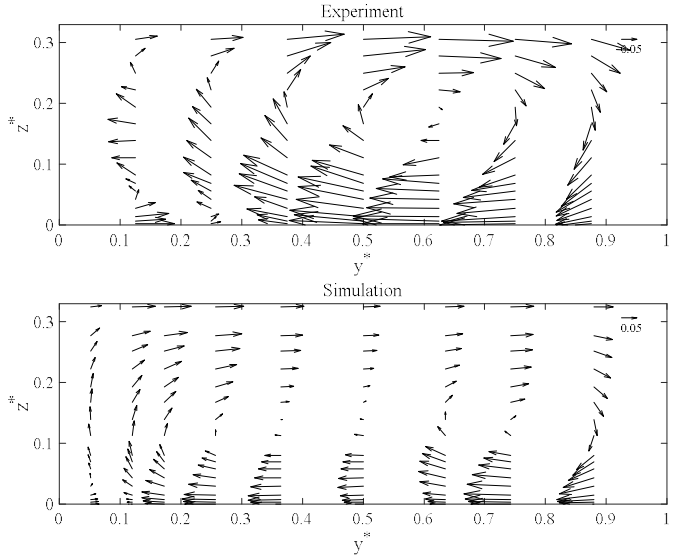

Figure 20. v*-w* velocity vector field q*=0.75 and when x* = 5

Moreover, the non-dimensional water depth contour plots divided by the upstream depth were drawn in Figure 21 and Figure 22 and it was observed that the depth decreases in the separation zones. The minimum depth ratios were investigated and they have generated the center of the separation zones. The minimum depth ratios were compared between the experiment and simulation. The simulation overestimated the minimum depth ratios, but they were validated against less than 1 percent error.

Furthermore, the longitudinal water depth profiles were plotted and compared in different y locations and they showed a great agreement as shown in Figure 23 and Figure 24, but the fluctuations in the separation zone were slightly larger in the simulation.

The non-dimensionalized turbulent kinetic energy by dividing the downstream velocity-squared was plotted in contour fields and compared with the experiment as described in Figure 25 and Figure 26. It was found that the kinetic energy is maximum around the separation zone and the maximum value of them increased as the discharge ratios increased. The turbulent kinetic energy showed a similar phenomenon that a single kinetic energy cloud was generated around the separation zone. However, small and multiple energy clouds were found in the experiment, whereas the simulation results presented a single cloud as the small discharge ratio result.

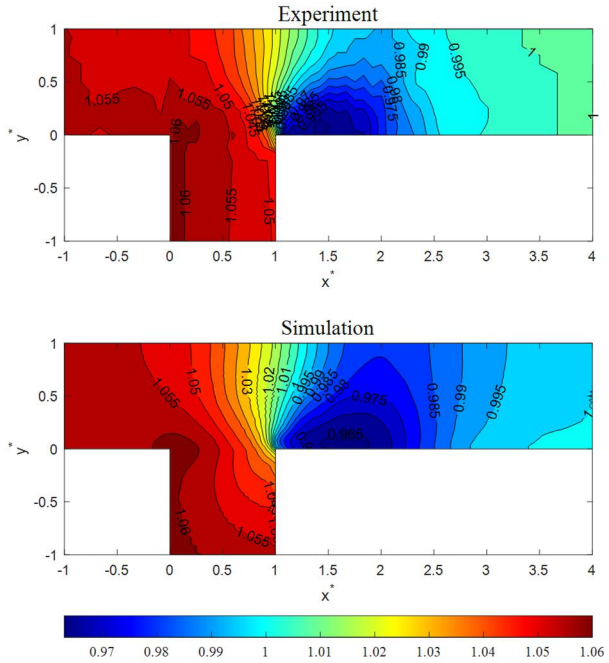

Figure 21. Non-dimensional water depth plot for q^{*}=0.25

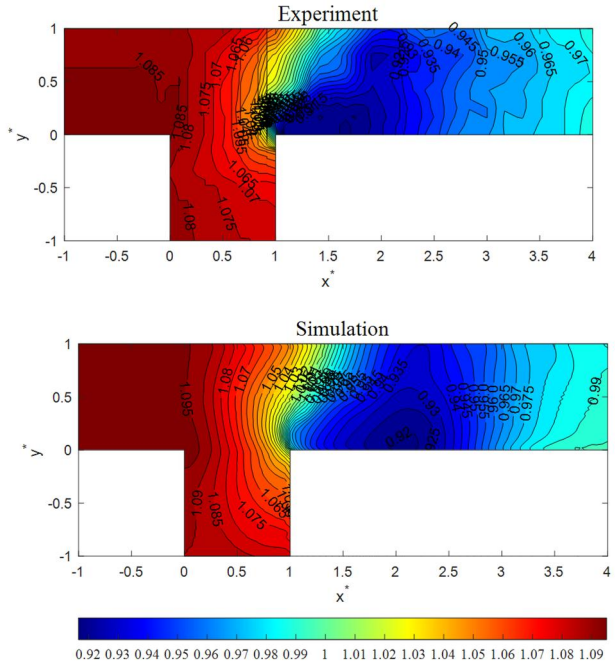

Figure 22. Non-dimensional water depth plot for q*=0.75

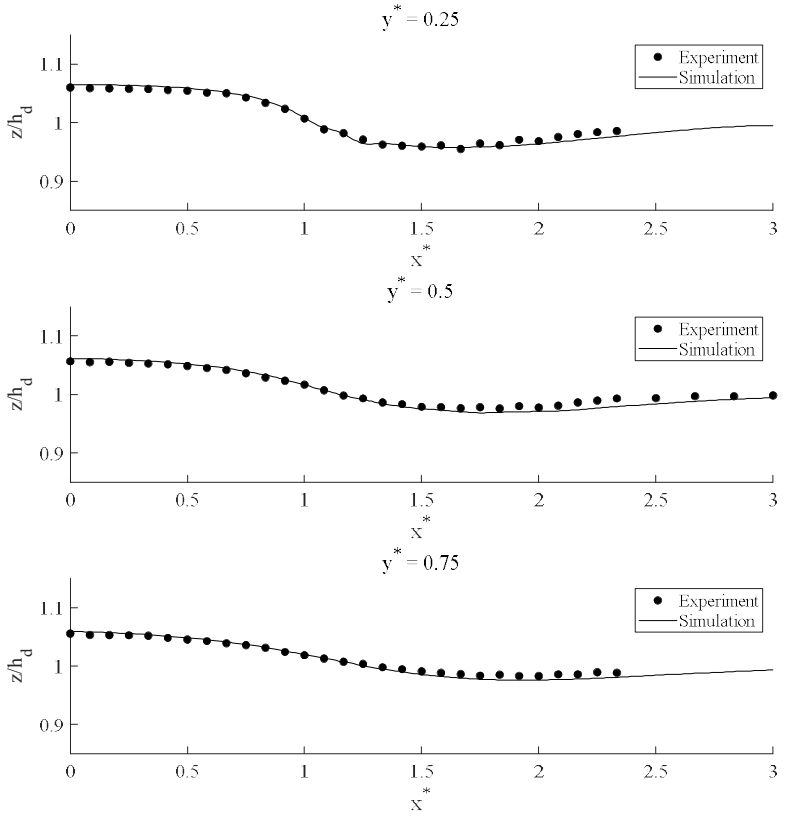

Figure 23. Longitudinal non-dimensional water depth plots for q*=0.25

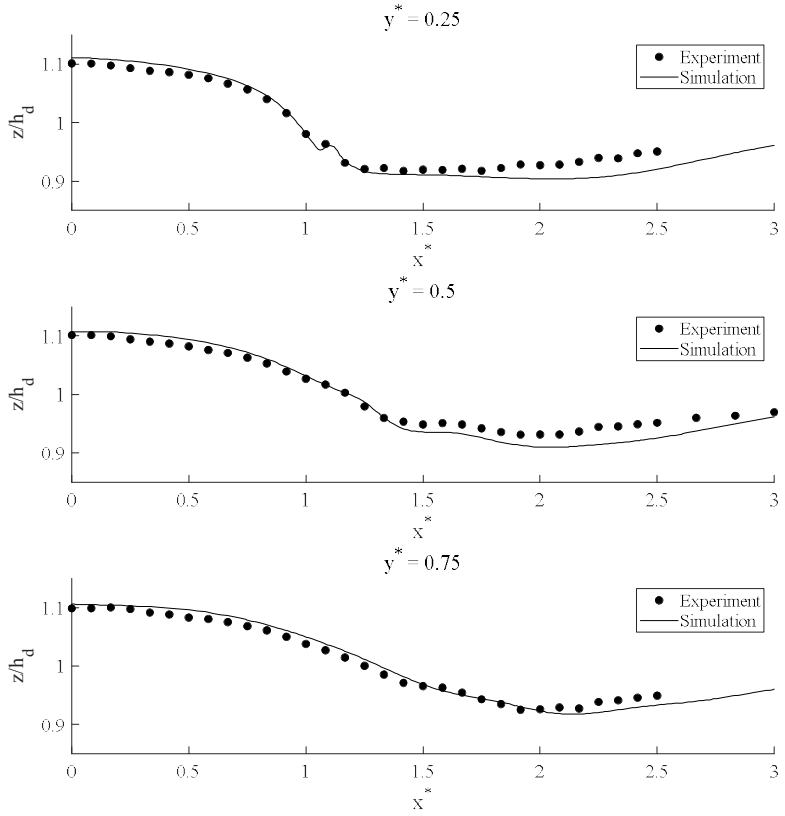

Figure 24. Longitudinal non-dimensional water depth plots for q*=0.75

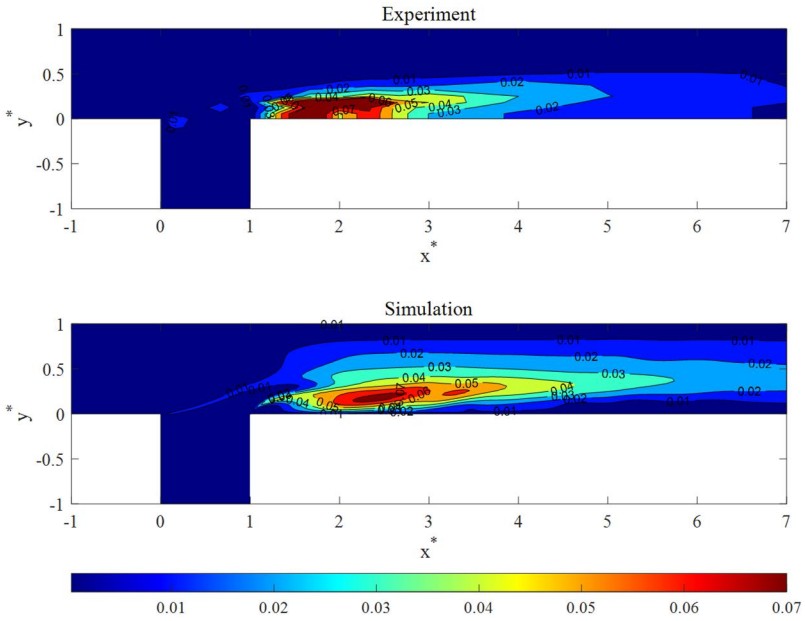

Figure 25. Non-dimensional turbulent kinetic energy for q*=0.25 at z* = 0.278

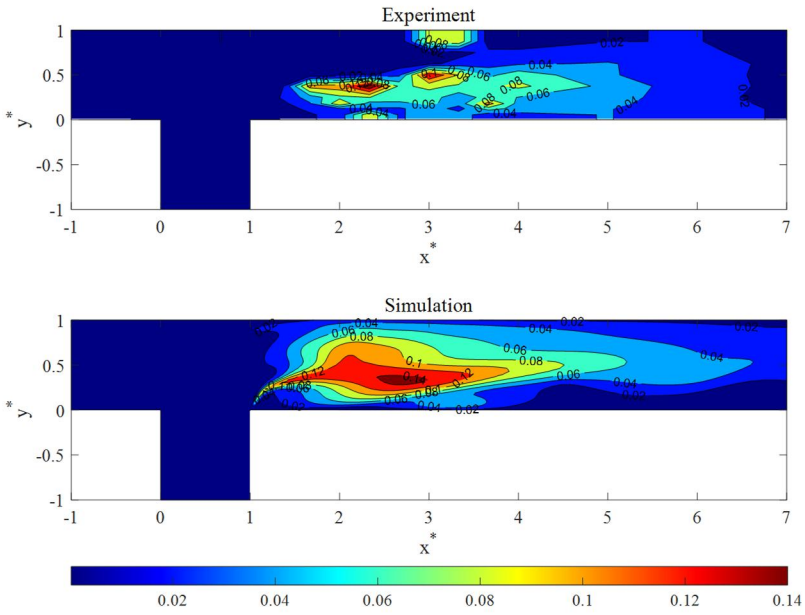

Figure 26. Non-dimensional turbulent kinetic energy for q*=0.75 at z* = 0.278

4.3 Discharge ratio and junction angle study with the experiment of Gurram et al. (1997)

The effect of both the discharge ratio and the junction angle and was simulated and validated against Gurram et al.'s experiment (1997). The discharge ratio was set to be 0.25, 0.5, and 0.75 and the Froude number is determined to be 0.5. The Reynolds number was $9.90*10^4$. The velocity plots in the x-direction at the water surface for 30, 60, and 90 degrees are described as seen in Figure 28, Figure 29, and Figure 30. The size of the separation zones increased as the discharge ratio and junction angle increased. The streamlines of them were drawn with the Line Integral Convolution (LIC) method to measure the specification of the separation zones to compare the results with Gurram et al.'s experiment results as shown in Figure 27. However, Yang et al. (2009) suggested the zero-velocity isovel measurement method which draws contour plots of u velocity and measures the size of the contour plot where u is zero. It is more convenient and efficient, but it tends to measure less than the streamline method.

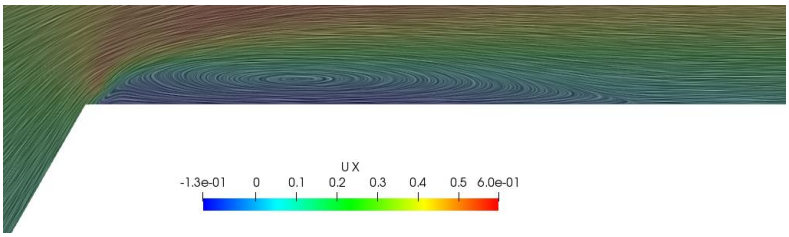

Figure 27. Streamline of the surface with 60 for q^*=0.25 drawn by Line Integral Convolution (LIC)

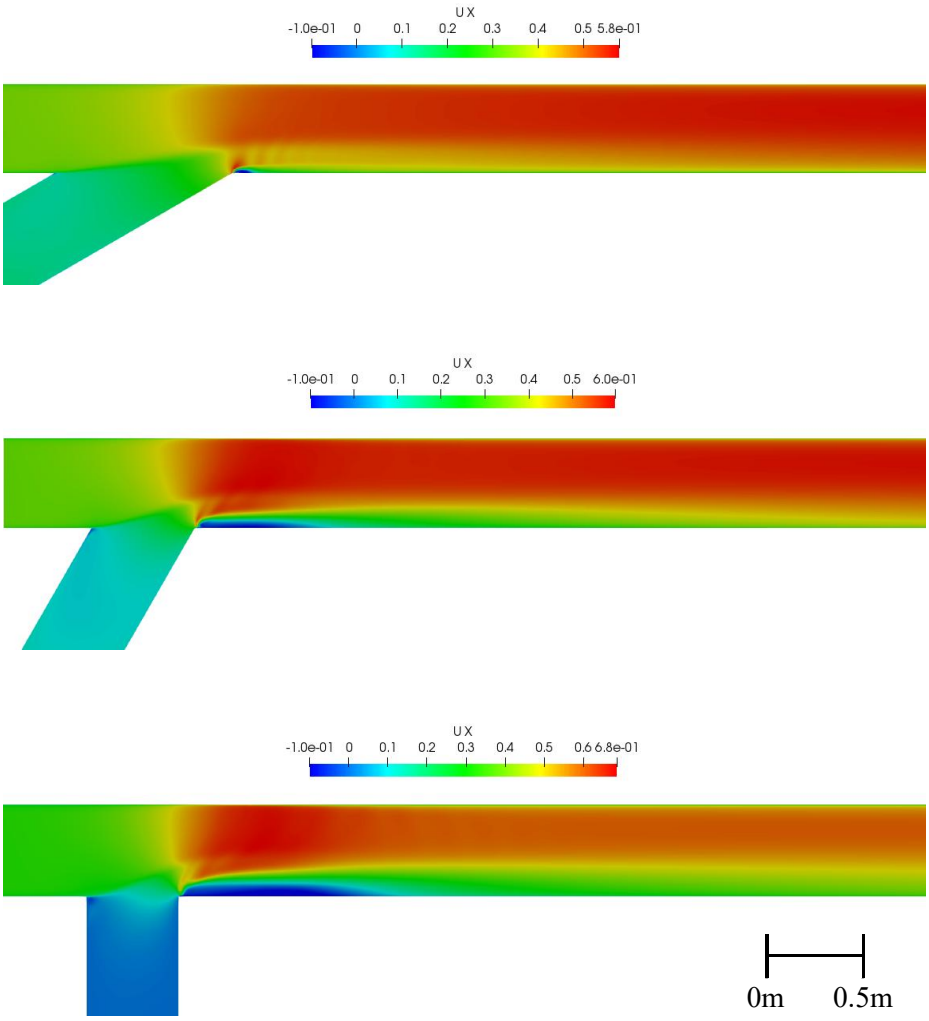

Figure 28. Surface u velocity fields with 30, 60, and 90 degrees for q^{*}=0.25

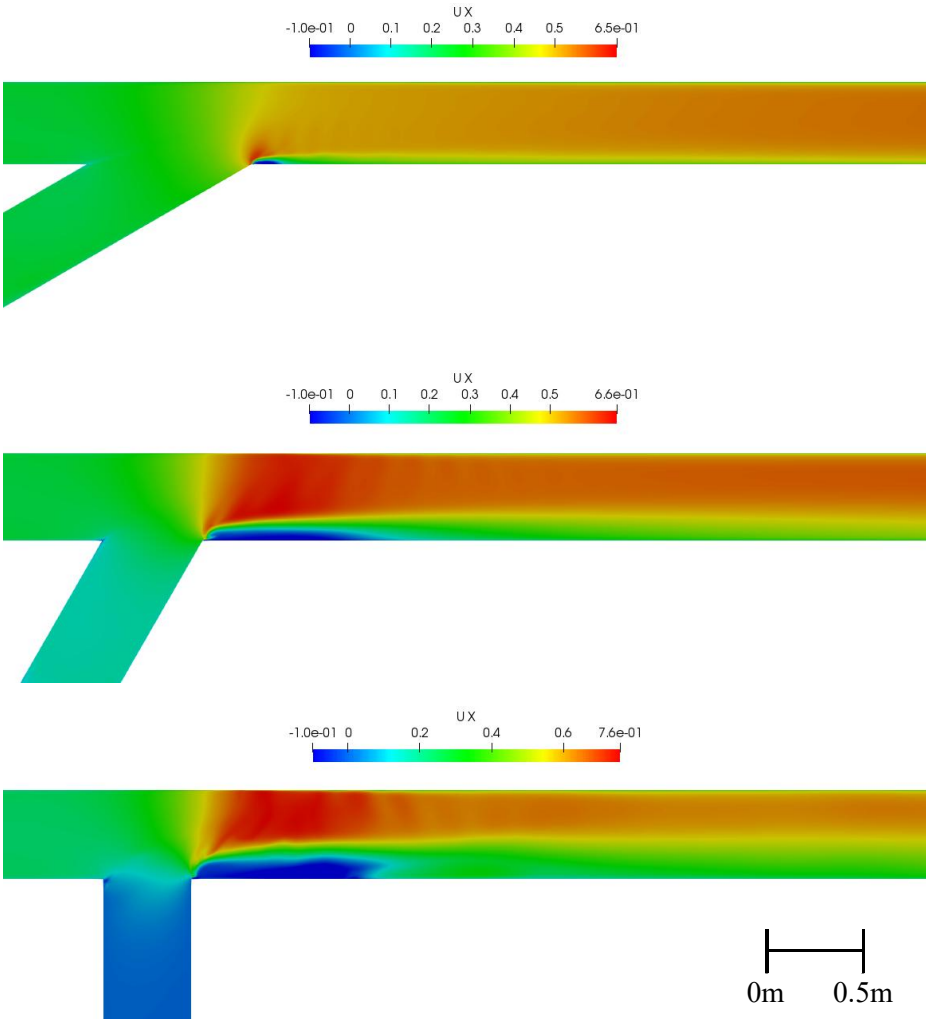

Figure 29. Surface u velocity fields with 30, 60, and 90 degrees for q^{*}=0.5

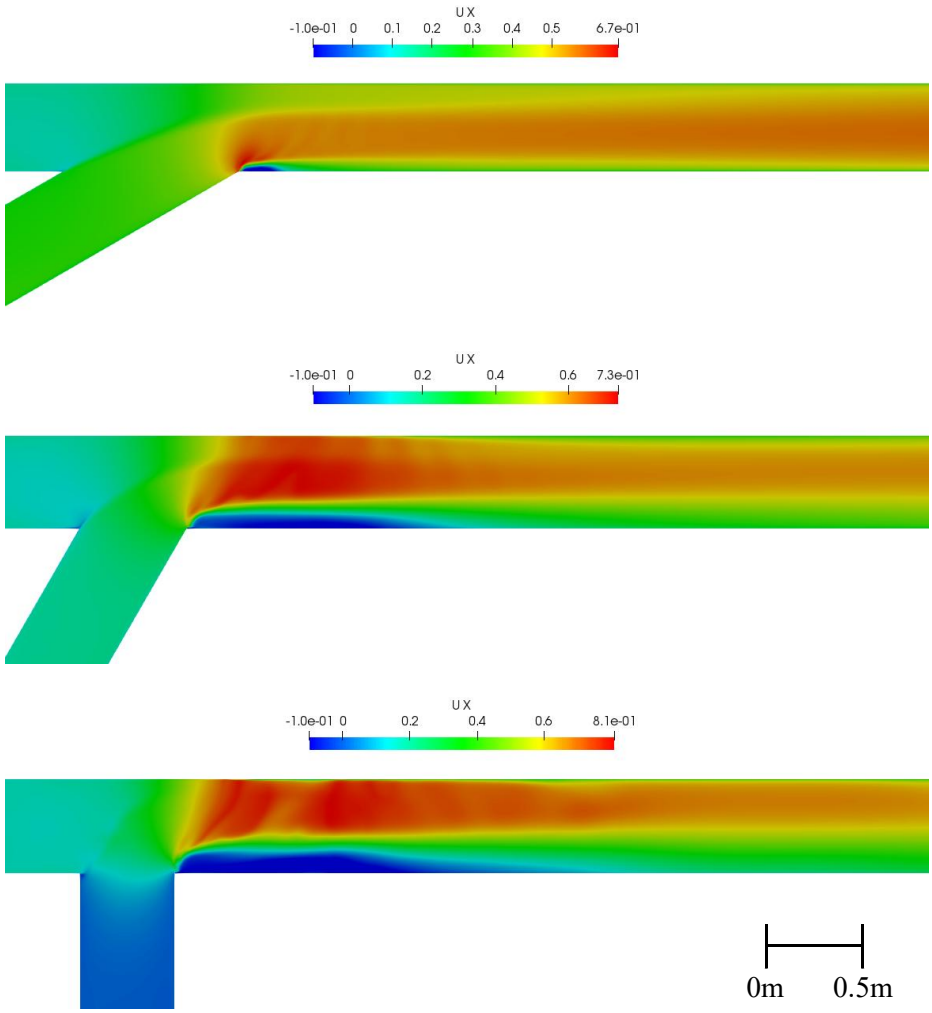

Figure 30. Surface u velocity fields with 30, 60, and 90 degrees for q^{*}=0.75

Furthermore, depth ratio changes were investigated in different discharge ratios and junction angles. It was found that the depth decreased around the separation zones. The size of the depth depression zone increased, and the minimum depth ratio decreased as the discharge ratio and junction angle increased since the separation zone got larger as shown in the figures.

Moreover, the turbulent kinetic energy results described that the maximum energy areas were formed above the separation zone. It was revealed that the maximum values tended to increase as the discharge ratios and junction angle increased since the turbulence rose as the flow accelerated.

Shear stress near the bed was calculated to predict the effect of the discharge ratio and junction angle on the bed morphology. it was observed that the maximum shear stress is generated above the separation zone and the magnitude and the size of them increase as the discharge ratio and junction angle increase as the experiments by Best (1998) and Luo et al. (2015) observed that the bed was eroded above the confluence zones, the shapes and sizes of them increased, and the bed morphology change increased as the discharge ratio and junction angle increased.

Besides, the v-w velocity vectors were illustrated to investigate the secondary flows with different discharge ratios and junction angles. Most secondary flows were developed after the separation zone, so the v-w vectors were plotted when x* is 5 and compared to each other. When the angle was 30 degrees, a clockwise secondary flow near the wall close to the junction had the

largest range among all the angles and it got larger when the discharge ratio increased. Furthermore, when the discharge ratio increased, another secondary flow was developed anticlockwise near the opposite walls. As the discharge ratio increased, the secondary flows by the shear layer tended to diminish since the lateral flow faced the walls before the orientation of the flow changed and the conflicted flow generated another the helical flows near the right wall.

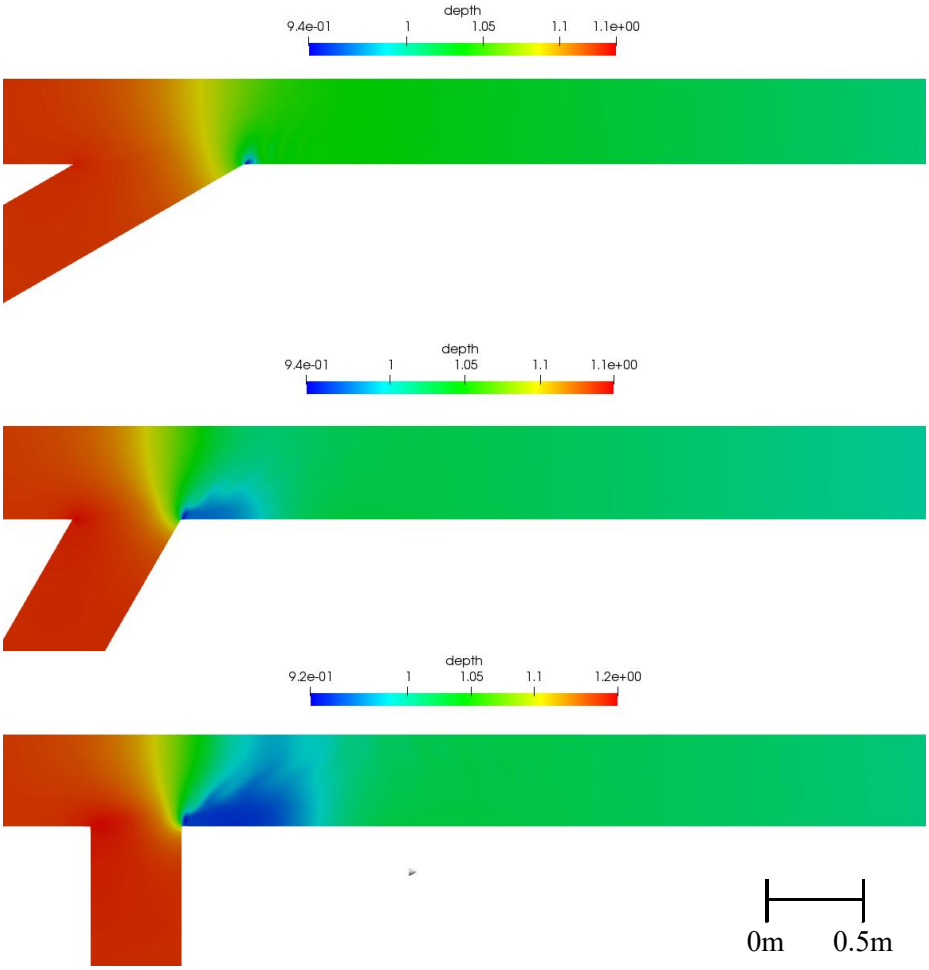

Figure 31. Depth ratios (h/h_d) with 30, 60, and 90 degrees for $q^*=0.25$

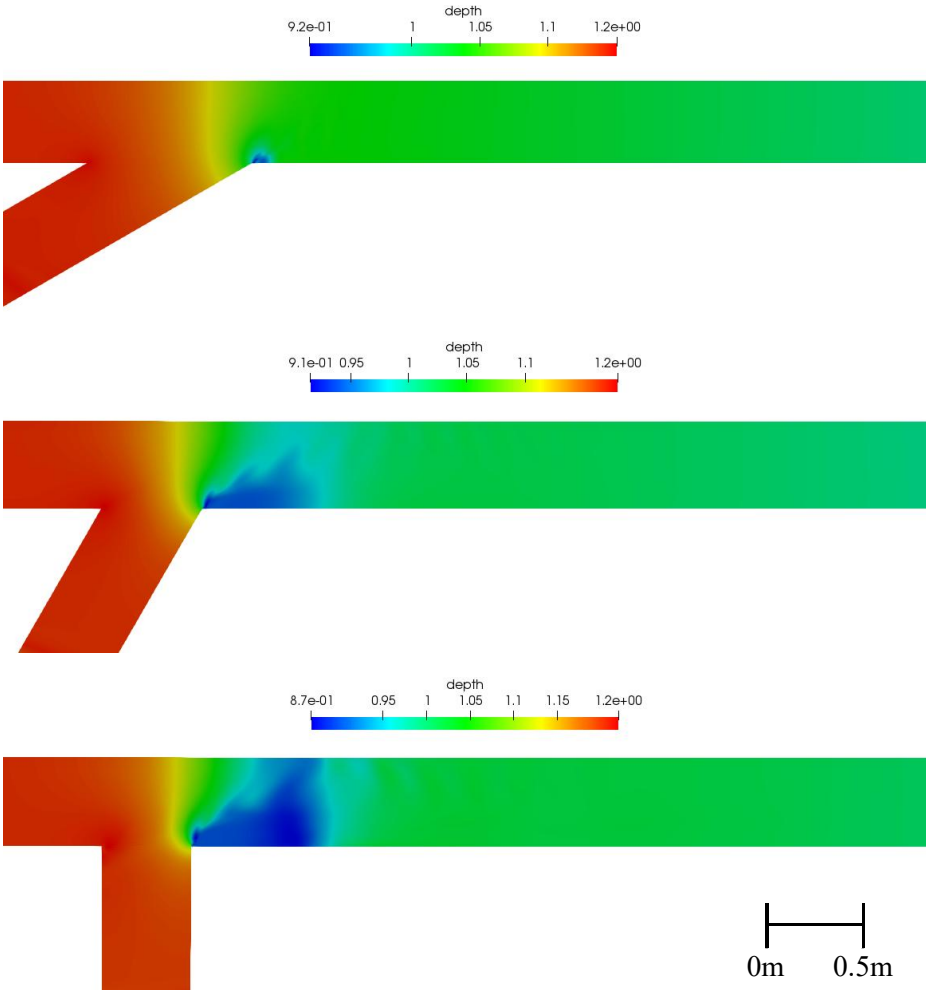

Figure 32. Depth ratios (h/h_d) with 30, 60, and 90 degrees for $q^*=0.5$

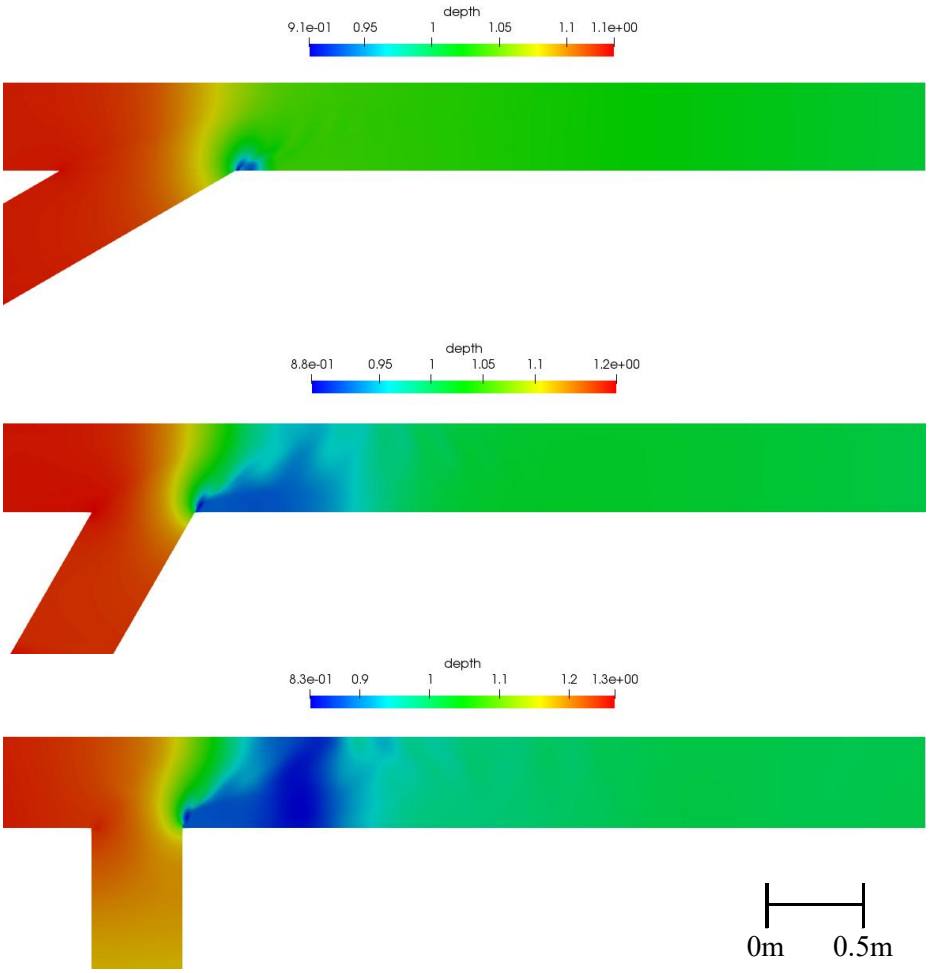

Figure 33. Depth ratios (h/h_d) with 30, 60, and 90 degrees for $q^*=0.75$

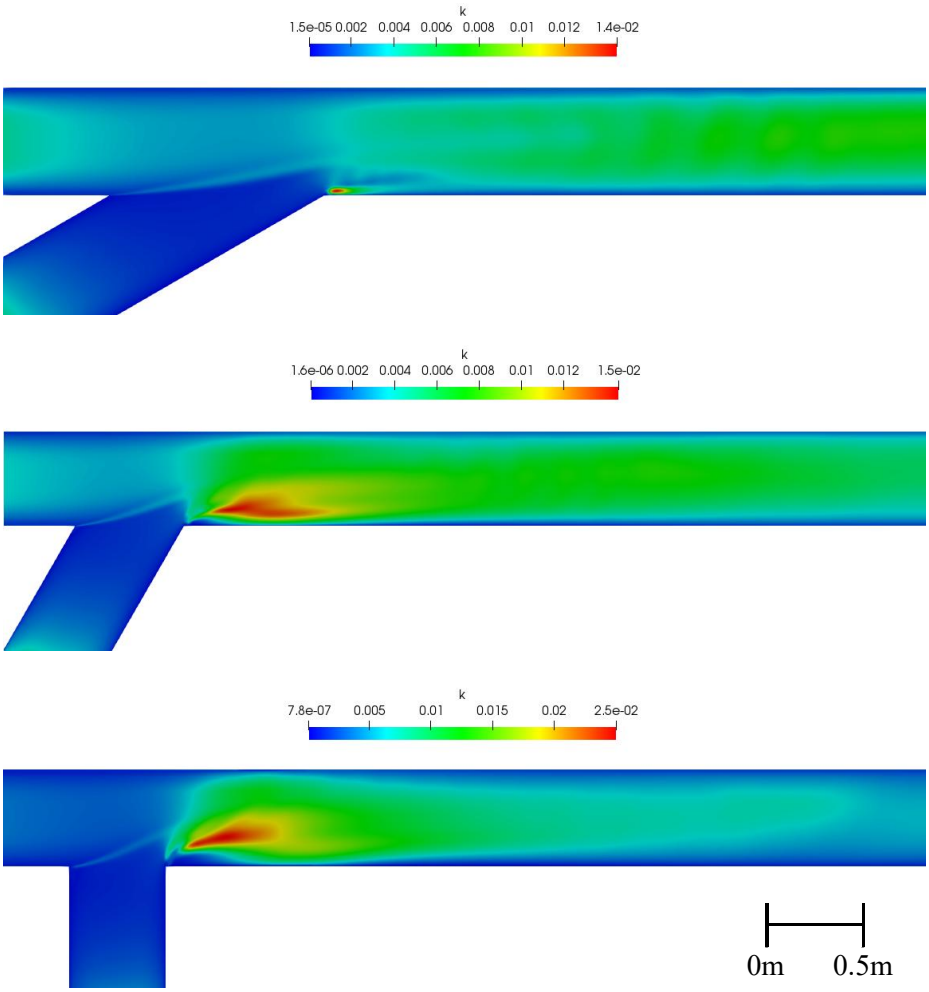

Figure 34. Turbulent kinetic energy on the surface with 30, 60, and 90 degrees for q^{*}=0.25

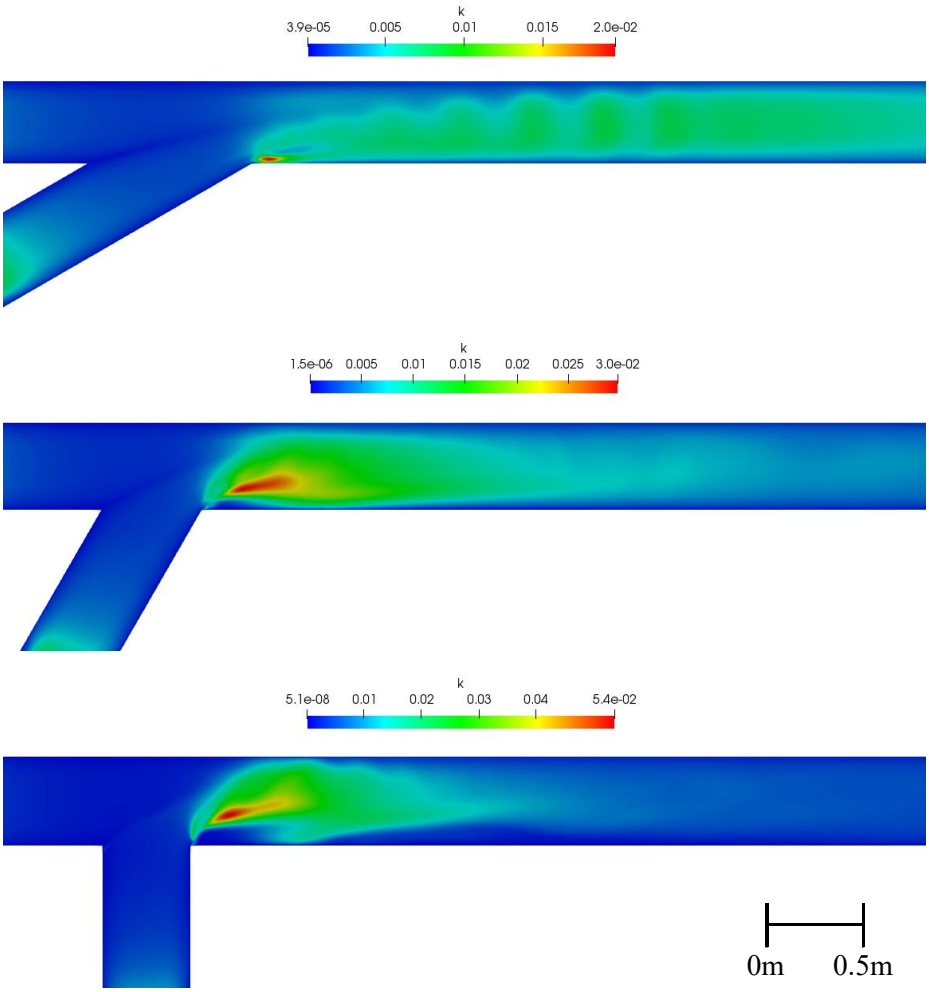

Figure 35. Turbulent kinetic energy on the surface with 30, 60, and 90 degrees for q^{*}=0.5

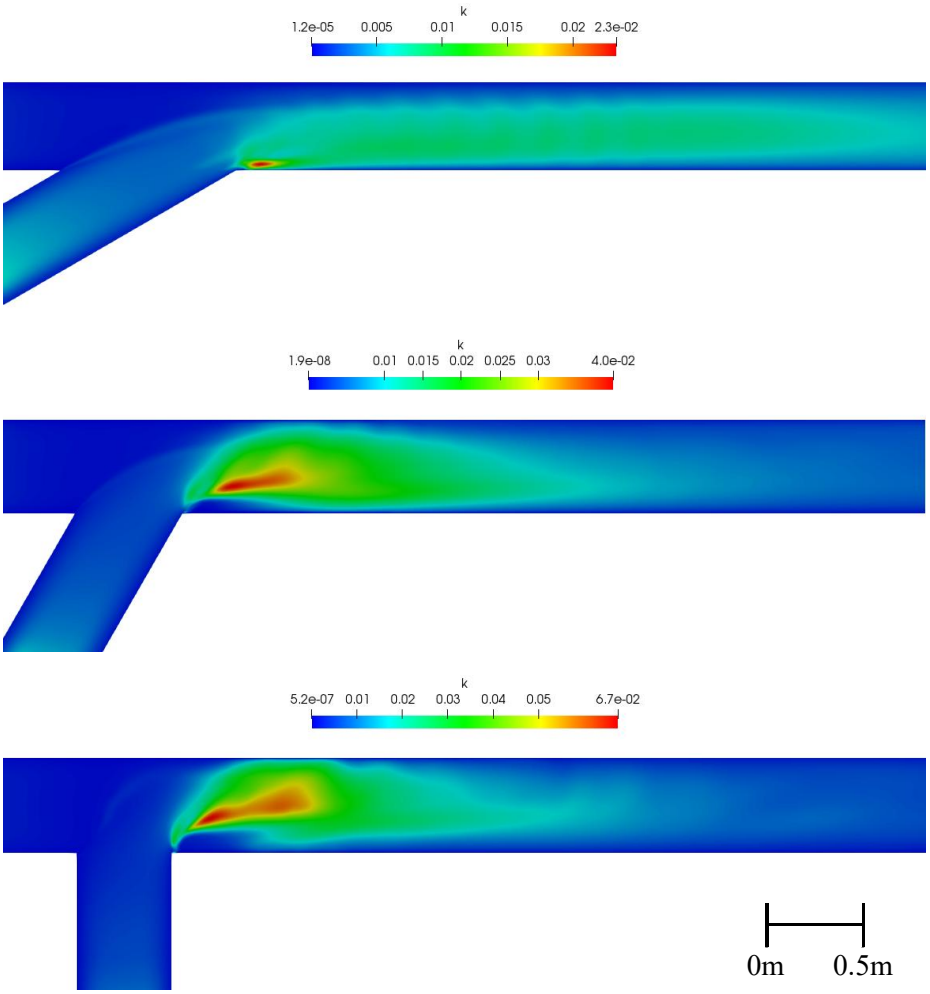

Figure 36. Turbulent kinetic energy on the surface with 30, 60, and 90 degrees for q^{*}=0.75

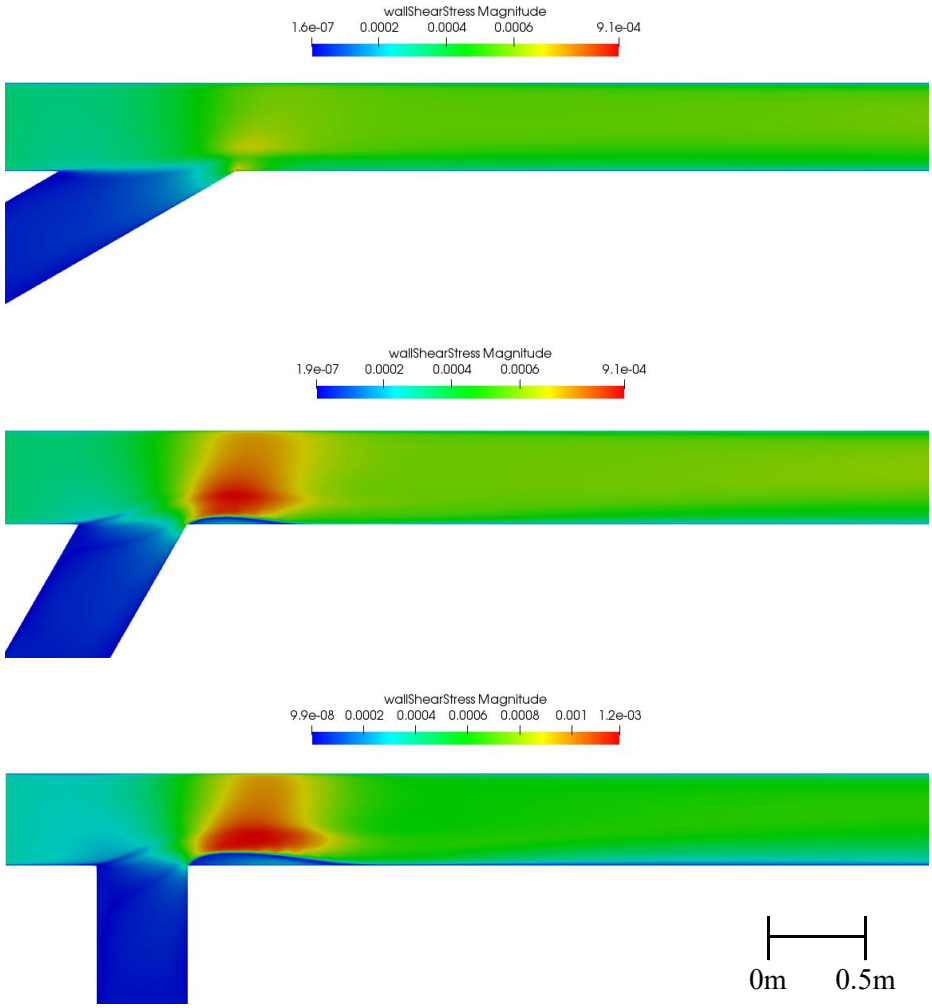

Figure 37. Wall shear stress near the bottom with 30, 60, and 90 degrees for q^{*}=0.25

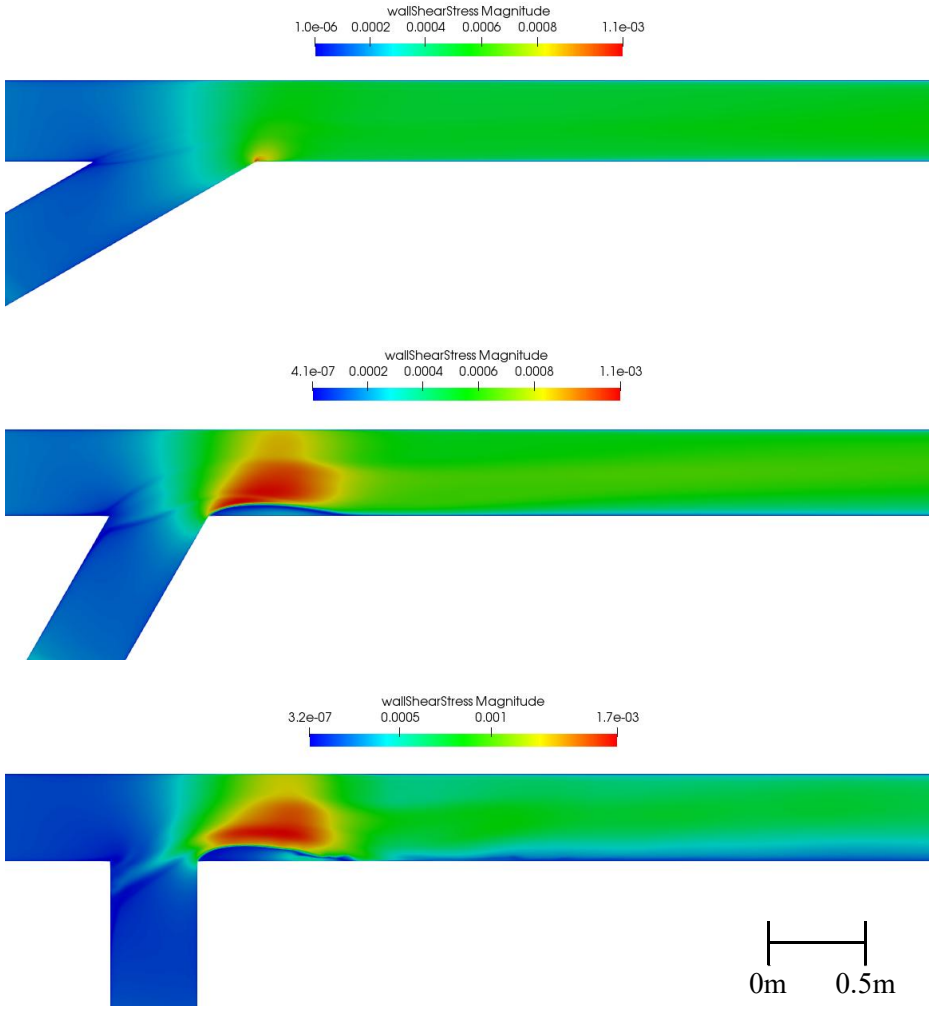

Figure 38. Wall shear stress near the bottom with 30, 60, and 90 degrees for q^{*}=0.5

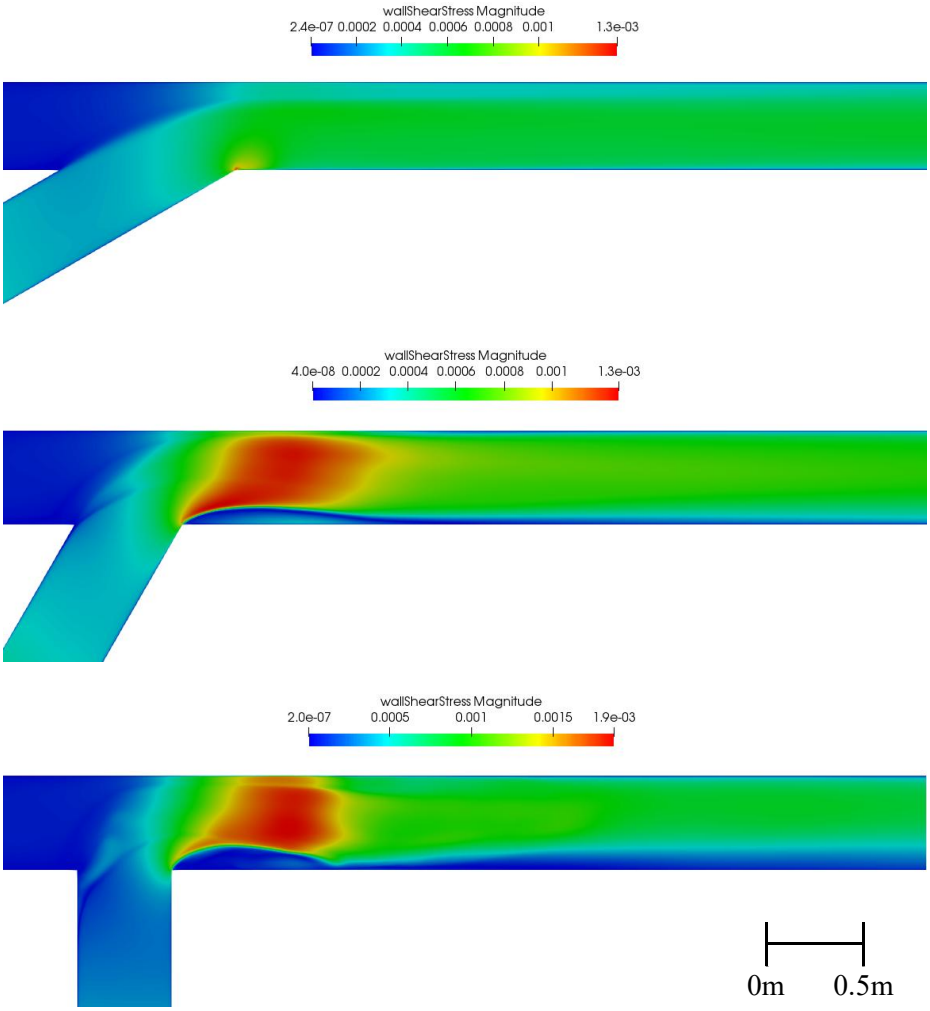

Figure 39. Wall shear stress near the bottom with 30, 60, and 90 degrees for q^{*}=0.75

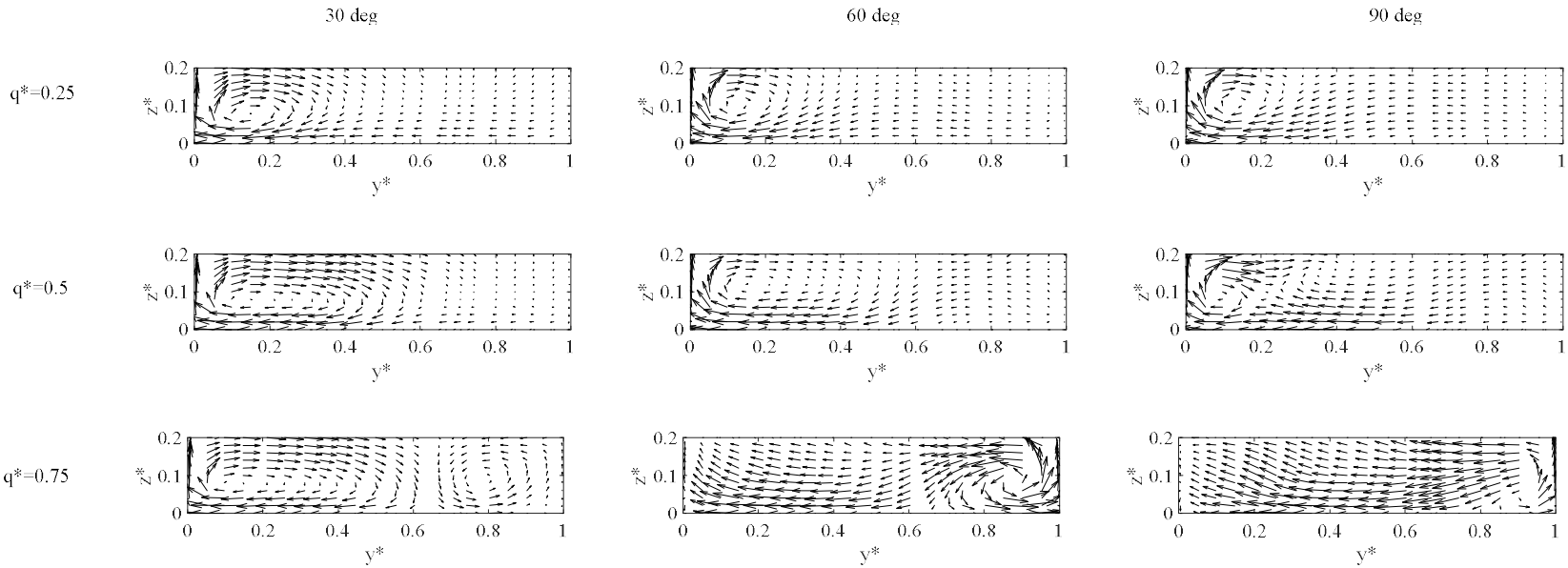

Figure 40. Secondary flows for each discharge ratio and junction angle for x* = 5

Numerical results based on Gurram et al.'s experiment (1997) of maximum width, $b_{s,}$ and length, l_s of the separation zones were compared to Gurram et al.'s experiment results as Figure 41 and Figure 42 describe. In general, they all indicated that the width and length of the separation zone increased as the discharge ratio and junction angle increase. The minimum error and maximum error of the width were 1.6 and 11.8 percent and those of the length were 0.4 and 15.8 percent respectively.

Some quantitative values of the simulation were presented below in order to see the relationship of them with the discharge ratio and junction angle even there was no validation data from the experiment.

The maximum u velocity results of the simulation were illustrated in Figure 43. It indicated that the maximum velocity and the rate of increase inclined as the discharge ratio and junction angle increased since they made flow contraction zone between the shear plane and the wall smaller and it caused higher flow acceleration above the separation zones.

Moreover, the maximum shear stress near the bed was plotted in Figure 44. and it was found that it grew as the discharge ratios and junction angle increased in general since the higher discharge ratio and junction angle developed the higher maximum velocity difference near the bed which caused higher shear stress. Besides, the maximum turbulent kinetic energy was presented in Figure 45. It tended to increase as the discharge ratio and junction angle increased

since they caused higher velocity around the separation zone and it induced higher turbulence. The rate of increase surged as the junction angle increased.

The minimum depth ratio (h/h_d) was investigated with various discharge ratios and junction angles. It was found that the minimum depth decreased as the discharge ratio and junction angle increased in general and the rate of decrease rose as the junction angle increased as shown in Figure 46.

Lastly, the maximum magnitudes of the secondary flows, $\sqrt{v^2 + w^2}$ when x* = 5 were presented in Figure 47. Generally, the maximum secondary flow magnitudes increased as the junction angle and discharge ratio increased. However, High discharge ratio and junction angle diminished the secondary flows while impinging the flow to the side walls. That caused less magnitudes of them when the discharge ratio is 0.75 and junction angles are 60 or 90 degrees.

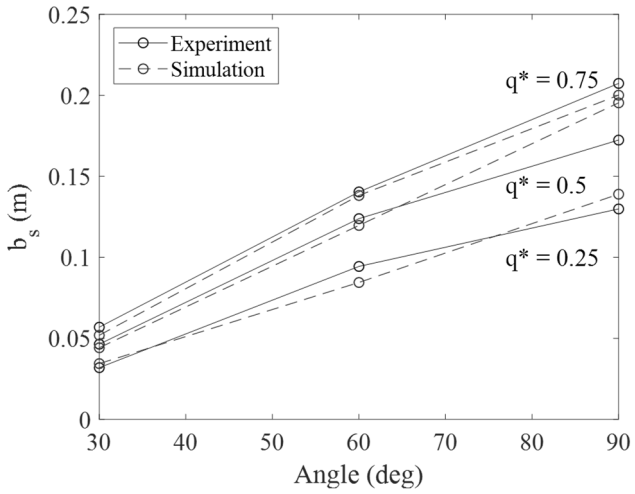

Figure 41. Comparison of the width of the separation zone with various discharge ratios and junction angles

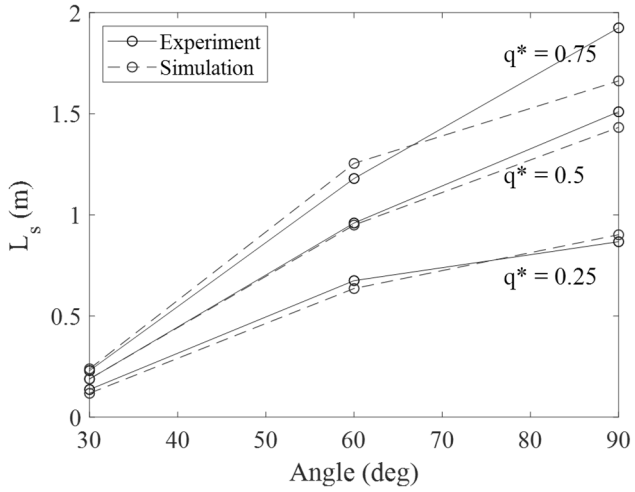

Figure 42. Comparison of the length of the separation zone with various discharge ratios and junction angles

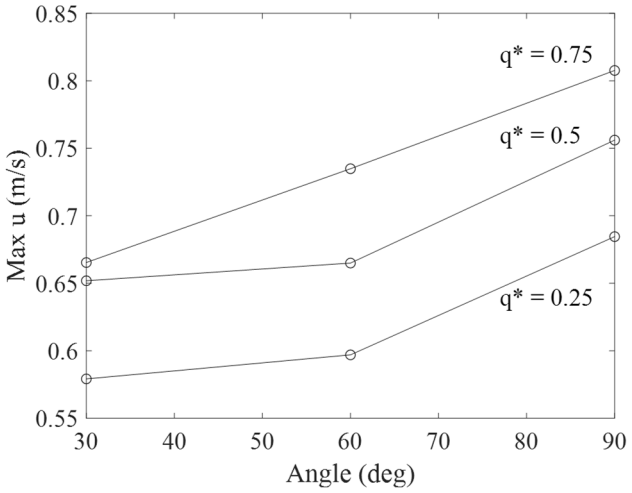

Figure 43. Maximum u velocity of simulation results with various discharge ratios and junction angles

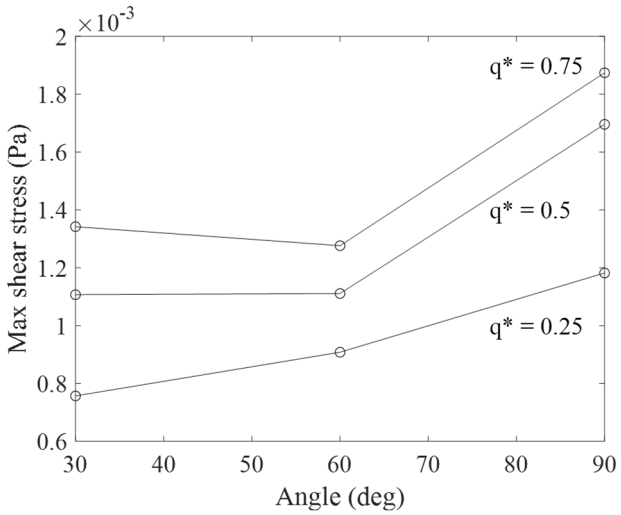

Figure 44. Maximum bed shear stress of simulation results with various discharge ratios and junction angles

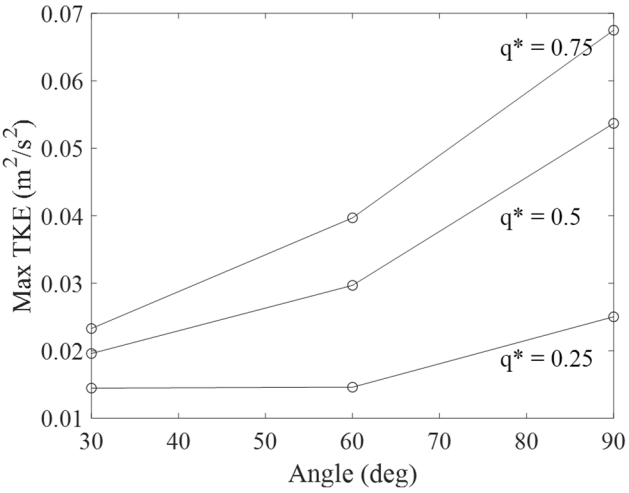

Figure 45. Maximum turbulent kinetic energy of simulation results with various discharge ratios and junction angles

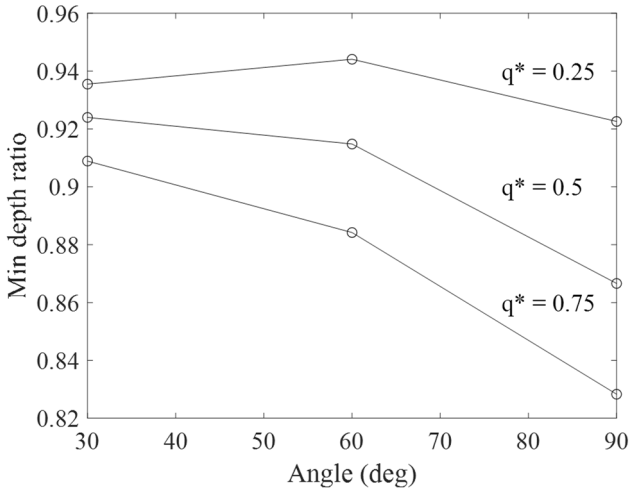

Figure 46. Minimum depth ratio (h/hd) of simulation results with various discharge ratios and junction angles

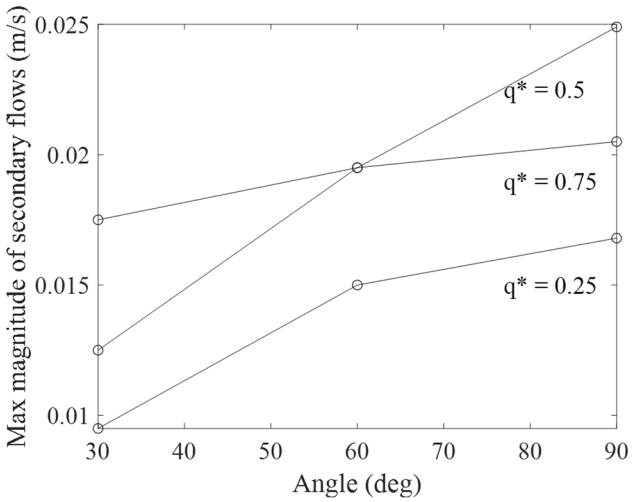

Figure 47. Maximum magnitude of the secondary flow of simulation results with various discharge ratios and junction angles

Mathematical modelling by Multiple Linear Regression (MLR) was conducted with the simulation results to simply estimate the flow characteristics including the width and length of the separation zone, maximum u velocity, maximum bottom shear stress, minimum depth ratio, and the maximum magnitude of secondary flow. The angle ratios that the junction angles were divided by 90 degrees and the discharge ratios were employed for this study to match the scales by non-dimensionalizing. The equation of MLR used for the analysis is presented below. The calculated adjusted R-squared values showed that the goodness-to-fit of the models. The minimum adjusted R-squared value of developed models was 0.787 for the maximum bottom shear stress and the maximum of that was 0.955 for the separation zone width. The mean squared errors were calculated in terms of the width and length of the separation zones using the numerical and experimental results. The results showed good estimation performance with 0.000136 and 0.0338 respectively.

However, it is obvious that the flow characteristics are non-linearly related to the discharge ratio and junction angle by more complex equations, and the number of samples was only nine, so it is necessary to have more values to convince these models.

$$y_i = \beta_0 + \beta_1 x_{i1} + \beta_2 x_{i2} + e \tag{17}$$

In addition, the sensitivity analysis using the Mean of the Partial Derivatives (MPD) verified that the separation zone varied more sensitively to the junction angle, whereas the other characteristics changed more sensitively to the

discharge ratio. It was interestingly found out that the MPD values were the same or close to the regression coefficients since the MPD implies the mean values of the slopes. This founding proposed the possibility that the Multiple Linear Regression can be employed for the sensitivity analysis if the characteristics showed linearities.

However, the number of the simulation results was not enough to validate these analyses comprehensively and the width and depth of the channel were not considered due to the large computational time. Thus, it seems necessary to conduct more cases of simulation with more discharge ratios, junction angles, widths, and water depths.

Table 8. Coefficients of the multiple linear regression models and the mean of the partial derivatives for each flow characteristic

	Separation zone width (m)	Separation zone length (m)	Maximum u velocity (m/s)	Maximum bottom shear stress (Pa)	Maximum turbulent kinetic energy (m^2/s^2)	Minimum depth ratio	Maximum magnitude of secondary flow (m/s)
β_0	-0.067	-0.832	0.449	0.000186	-0.023	1.014	0.00429
β_1 (angle*)	0.202	1.727	0.176	0.000773	0.044	-0.075	0.0114
β_2 (q*)	0.088	1.003	0.231	0.00110	0.051	-0.121	0.0108
Adjusted R-squared	0.983	0.960	0.969	0.921	0.924	0.916	0.704
MPD (angle*)	0.202	1.728	0.176	0.000838	0.0444	0.0840	0.0114
MPD (q*)	0.088	1.003	0.231	0.001097	0.0509	0.1205	0.0166

Chapter 5. Conclusion

A three-dimensional numerical study was conducted to investigate the effects of the discharge ratios and junction angles at the confluent flow characteristics by OpenFOAM CFD software with SST k-ω turbulence model and Volume of Fluid (VOF) method.

Firstly, the gird independence study was conducted, and it was found out that the mesh with approximately 2760000 cells was fine enough to result in the convergence against the number and size of cells.

Secondly, the numerical investigation with different discharge ratios was carried out based on the experiment by Shumate (1998) and the results were comprehensively validated against the point data of the experiment. The simulation result showed a reasonably good agreement with the experiment data by the contour, vector, and profile plots. It was revealed that the separation zone, the maximum velocity, flow angle, maximum kinetic energy, maximum increased as the discharge ratio rose, but the size of the maximum velocity and the minimum depth ratio as the discharge ratio increased.

Thirdly, numerical investigation with various discharge ratios and junction angles based on the experiment by Gurram et al. (1997) was carried out and quantitative validations in terms of separation zones were conducted with the experimental data. The width and length of the separation zone were validated against less than 16 percent. It was verified that the separation zone, the

maximum velocity, maximum turbulent kinetic energy, maximum bottom shear stress, the depth depression zone, and maximum magnitude of secondary flow increased, and the minimum depth ratio decreased while the discharge ratio and junction angle increased in general.

Lastly, mathematical models were developed by Multiple Linear Regression analysis to provide the simple estimation of the flow characteristics, and the correlation analysis was conducted to investigate the relationship of the discharge ratios and junction angles to the flow characteristics. The developed models provide a high goodness-of-fit with the high adjusted R-squared and high prediction with low MSE values. the sensitivity analysis using the mean of the partial derivatives verified that the separation zone varied more sensitively to the junction angle, whereas the other characteristics changed more sensitively to the discharge ratio.

However, the other quantitative characteristics except the width and length separation zone were not validated due to the absence of the experimental data. The number of simulation cases was not enough for comprehensive validation and the effect of the width and depth of the channels was not considered due to the high computational time. Thus, it is necessary to conduct a greater number of simulations with different discharge ratios, junction angles, channel width, and depth in order to prove the validity of the simulation results and apply the mathematical models to different geometries.

References

Ahn, S. S., Moon, S. C., Park, D. I., & Kim Jung, K. (2014). Analysis of flow characteristics in channel junction river. *Korean Society of Civil Engineers Convention.* 895 – 896.

Ahn, S. S., Yim, D. H., Jung, D. J., & Choi, S. C. (2006). Numerical analysis of the flow around channel junctions. *Korean Society of Civil Engineers Convention*. 1903-1906.

Best, J. L. (1988). Sediment transport and bed morphology at river channel confluences. *Sedimentology, 35*(3), 481-498.

Best, J. L., & Reid, I. (1984). Separation zone at open-channel junctions. *Journal of Hydraulic Engineering, 110*(11), 1588-1594.

Birjukova, O., Guillén Ludeña, S., Alegria, F., & Cardoso, A. H. (2014). Three-dimensional flow field at confluent fixed-bed open channels. *River flow.*

Biron, P., Best, J. L., & Roy, A. G. (1996). Effects of bed discordance on flow dynamics at open channel confluences. *Journal of Hydraulic Engineering, 122*(12), 676-682.

Biron, P. M., Ramamurthy, A. S., & Han, S. (2004). Three-dimensional numerical modeling of mixing at river confluences. *Journal of Hydraulic*

Engineering, 130(3), 243-253.

Biswal, S., Mohapatra, P., & Muralidhar, K. (2010). Flow separation at an open channel confluence. *Journal of Hydraulic Engineering, 16*(sup1), 89-98.

Bonakdari, H., Lipeme-Kouyi, G., & Wang, X. (2011). Experimental validation of CFD modeling of multiphase flow through open channel confluence. Paper presented at *the World Environmental and Water Resources Congress 2011*: Bearing Knowledge for Sustainability.

Bradbrook, K., Lane, S., Richards, K., Biron, P., & Roy, A. (2001). Role of bed discordance at asymmetrical river confluences. *Journal of Hydraulic Engineering, 127*(5), 351-368.

Cho, H.-K. (2007). A study on the hydraulic characteristics of river junctions using FLDWAV model. *Journal of The Korean Society of Industry Convergence, 10*(4), 275-283.

Cho, M. S., Choi, H. S., & Moon, h. g. (2006). Analysis of hydraulic characteristics at confluence by lateral inflow. *Journal of the Korean Society of Hazard Mitigation*, *6*(1), 59-68.

Choi, G. W., & Kang, G. (1993). 하천 합류점에서 합류각도에 따른 흐름해석. *Journal of The Korean Society of Civil Engineers 2,* 127-130.

Choi, G. W., Kim, G. H., & Cho, J. B. (2004). Analysis for the flow characteristics at natural channel junction by hydraulic model test. *Korean Society of Civil Engineers Convention,* 928-933.

Choi, G. W., Kim, G. H., Cho, J. B., & Kim, Y. K. (2004). The comparisons of the characteristics at channel junction between natural river section and rectangular channel section. *Korean Society of Civil Engineers Convention,* 3369-3373.

Choi, G. W., Kim, Y. K., & Jin, Y. Y. (2003). Changing of channel bed through discharge ratio at junction. *Korean Society of Civil Engineers Convention,* 2439-2442.

Choi, G. W., Lee, H. S., Han, H. J., & Chung, Y. J. (2004). The analysis of channel junction flow Nam-Han river to the 2-dimension. *Korean Society of Civil Engineers Convention,* 3299-3303.

Choi, G. W., Park, Y. S., & Han, M. S. (2003). The analysis of hydraulic characteristics at channel junctions through hydraulic model tests. *Korean Society of Civil Engineers Convention,* 2816-2821.

Choi, G. W., Park, Y. S., & Han, M. S. (2003). The change of flow depending upon the discharge and approaching angle at channel junctions. *Korean Society of Civil Engineers Convention,* 2835-2840.

Choi, H. S., Cho, M. S., & Park, Y. S. (2006). Analysis of flood characteristics at confluence by lateral inflow. *Journal of the Korean Society of Hazard Mitigation, 6*, 59-68.

Creëlle, S., Schindfessel, L., Cunha Ramos, P., & De Mulder, T. (2016). Experimental investigation of the flow evolution in the tributary of a 90 open

channel confluence. *River Flow 2016*.

Davidson, J., Cathelain, M., Guillemet, L., Le Huec, T., & Ringwood, J. (2015). Implementation of an openfoam numerical wave tank for wave energy experiments. *Proceedings of the 11th European wave and tidal energy conference*.

Đorđević, D. (2012). Numerical study of 3D flow at right-angled confluences with and without upstream planform curvature. *Journal of Hydraulic Engineering, 15*(4), 1073-1088.

Foundation, T. O. (Producer). (2019). OpenFOAM v5 User Guide: 4.5 Solution and algorithm control.

Ghostine, R., Kesserwani, G., Mose, R., Vazquez, J., Ghenaim, A., & Gregoire, C. (2009). A confrontation of 1D and 2D RKDG numerical simulation of transitional flow at open-channel junction. *International journal for numerical methods in fluids, 61*(7), 752-767.

Ghostine, R., Vazquez, J., Terfous, A., Rivière, N., Ghenaim, A., & Mosé, R. (2013). A comparative study of 1D and 2D approaches for simulating flows at right angled dividing junctions. *Applied Mathematics computation, 219*(10), 5070-5082.

Gurram, S. K., Karki, K. S., & Hager, W. H. (1997). Subcritical junction flow. *Journal of Hydraulic Engineering, 123*(5), 447-455.

Hager, W. H. (1987). Discussion of "Separation Zone at Open-Channel

Junctions” by James L. Best and Ian Reid (November 1984). *Journal of Hydraulic Engineering, 113*(4), 539-543.

Hsu, C.-C., Lee, W.-J., & Chang, C.-H. (1998). Subcritical open-channel junction flow. *Journal of Hydraulic Engineering, 124*(8), 847-855.

Hsu, C.-C., Wu, F.-S., & Lee, W.-J. (1998). Flow at 90 equal-width open-channel junction. *Journal of Hydraulic Engineering, 124*(2), 186-191.

Huang, J., Weber, L. J., & Lai, Y. G. (2002). Three-dimensional numerical study of flows in open-channel junctions. *Journal of Hydraulic Engineering, 128*(3), 268-280.

Jang, C.-L., Kim, J.-T., Park, B.-J., & Yum, K. (2007). 낙동강과 금호강 합류부 구간에서 유입유량에 따른 흐름 및 하상변동 특성 변화에 관한 수치모의 연구. *Korean Society of Civil Engineers Convention*, 4124-4128.

Japan, M. (Producer). (2018). 'Backwater phenomenon' linked to deadly flood in Okayama Pref.: experts.

Ji, U., & Jang, E.-K. (2017). Numerical analysis on flow and bed change characteristics by discharge variations at the confluence of Nakdong and Geumho rivers. *Journal of the Korea Academy-Industrial Cooperation Society 18*(12), 659-667.

Kasthuri, B., & Pundarikanthan, N. (1987). Discussion of “Separation zone at open-channel junctions” by Kames L. best and Ian Reid (November 1984).

Journal of Hydraulic Engineering, 113(4), 543-544.

Kim, G., & Choi, G. W. (2006). Analysis for difference of water surface elevation at cross section in Pyungchang river contained junction using hydraulic model. *Journal of the Korean Society of Hazard Mitigation, 6*, 57-65.

Kim, J. S., Kim, K. S., Kim, W., & Kim, S. H. (2009). Analysis of flood stage in a confluence using the dynamic numerical model. *Journal of The Korean Society of Civil Engineers B, 29*(5B), 453-461.

Kwak, S. J., & Rhee, D. S. (2012). Preliminary study on the stage variation following inflow and angles of confluence changes at the confluence. *Korean Society of Civil Engineers Convention*, 1751-1754.

Lee, J. (2013). Experimental investigation of flow characteristics in a confluent channel with bed elevation difference. (Master's degree), Seoul National University.

Lin, J., & Soong, H. (1979). Junction losses in open channel flows. *Water Resources Research, 15*(2), 414-418.

Liu, T., Fan, B., & Lu, J. (2015). Sediment–flow interactions at channel confluences: A flume study. *Advances in Mechanical Engineering*, *7*(6), 1687814015590525.

Luo, H., Fytanidis, D. K., Schmidt, A. R., & García, M. H. (2018). Comparative 1D and 3D numerical investigation of open-channel junction

flows and energy losses. *Advances in water resources, 117*, 120-139.

Menter, F. R. (1994). Two-equation eddy-viscosity turbulence models for engineering applications. *AIAA journal, 32*(8), 1598-1605.

Pinto Coelho, M. M. L. (2015). Experimental determination of free surface levels at open-channel junctions. *Journal of Hydraulic Research, 53*(3), 394-399.

Press, J. (Producer). (2018). An aerial view of flooded houses in Kurashiki, Okayama Prefecture, Japan, on July 8, 2018.

Qing-Yuan, Y., Xian-Ye, W., Wei-Zhen, L., & Xie-Kang, W. (2009). Experimental study on characteristics of separation zone in confluence zones in rivers. *Journal of Hydrologic Engineering, 14*(2), 166-171.

Ramamurthy, A. S., Carballada, L. B., & Tran, D. M. (1988). Combining open channel flow at right angled junctions. *Journal of Hydraulic Engineering, 114*(12), 1449-1460.

Rice, S. P., Kiffney, P., Greene, C., & Pess, G. R. (2008). The ecological importance of tributaries and confluences. In *River confluences, tributaries the fluvial network*, 209-242.

Seo, I. W., & Park, I. (2013). Determination of ecological flow at the confluence of nakdong river and gumho river using river2d. *Journal of The Korean Society of Civil Engineers, 33*(3), 947-956.

Shakibainia, A., Tabatabai, M. R. M., & Zarrati, A. R. (2010). Three-

dimensional numerical study of flow structure in channel confluences. *Canadian Journal of Civil Engineering, 37*(5), 772-781.

Sharifipour, M., Bonakdari, H., Zaji, A. H., & Shamshirband, S. (2015). Numerical investigation of flow field and flowmeter accuracy in open-channel junctions. *Engineering Applications of Computational Fluid Mechanics, 9*(1), 280-290.

Shumate, E. D. (1998). Experimental description of flow at an open-channel junction. (MS thesis), University of Iowa.

Sivakumar, M., Dissanayake, K., & Godbole, A. (2004). Numerical modeling of flow at an open-channel confluence. *the Environmental Engineering Research Event*, Australia.

Song, C. G. "Finite Element Model for Shallow Water Flow Incorporating Dispersion Stresses and Generalized BCs." (2011). (Doctor's degree), Seoul National University.

Wang, X., Wang, X., Lu, W., & Liu, T. (2007). Experimental study on flow behavior at open channel confluences. *Frontiers of Architecture Civil Engineering in China, 1*(2), 211-216.

Webber, N. B., & Greated, C. (1966). An investigation of flow behaviour at the junction of rectangular channels. *Proceedings of the Institution of Civil Engineers, 34*(3), 321-334.

Weber, L. J., Schumate, E. D., & Mawer, N. (2001). Experiments on flow at a

90 open-channel junction. *Journal of Hydraulic Engineering, 127*(5), 340-350.

Yang, Q., Liu, T., Lu, W., & Wang, X. (2013). Numerical simulation of confluence flow in open channel with dynamic meshes techniques. *Advances in Mechanical Engineering, 5*, 860431.

Yuan, S., Tang, H., Xiao, Y., Qiu, X., Zhang, H., & Yu, D. (2016). Turbulent flow structure at a 90-degree open channel confluence: Accounting for the distortion of the shear layer. *Journal of hydro-environment research, 12*, 130-147.

Zhang, T., Xu, W.-l., & Chao, W. (2009). Effect of discharge ratio on flow characteristics in 90 equal-width open-channel junction. *Journal of Hydrodynamics, 21*(4), 541-549.

Appendix A. v*-w* vector plots of Shumate (1998)

q* = 0.25

x*=0

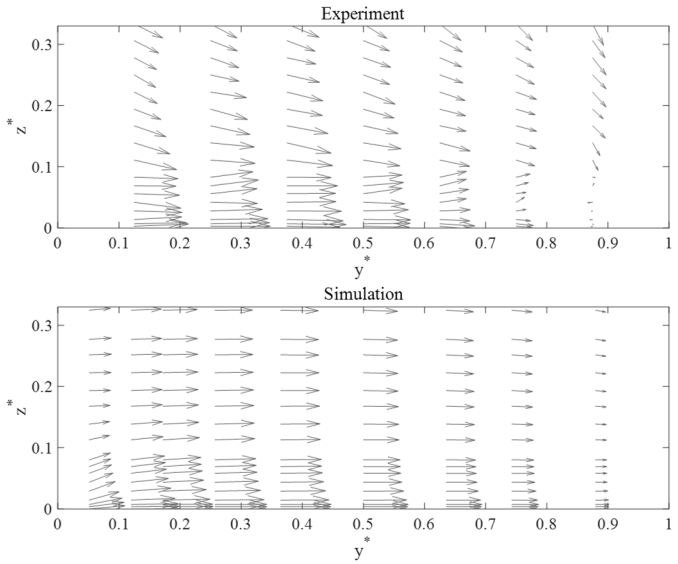

x*=1

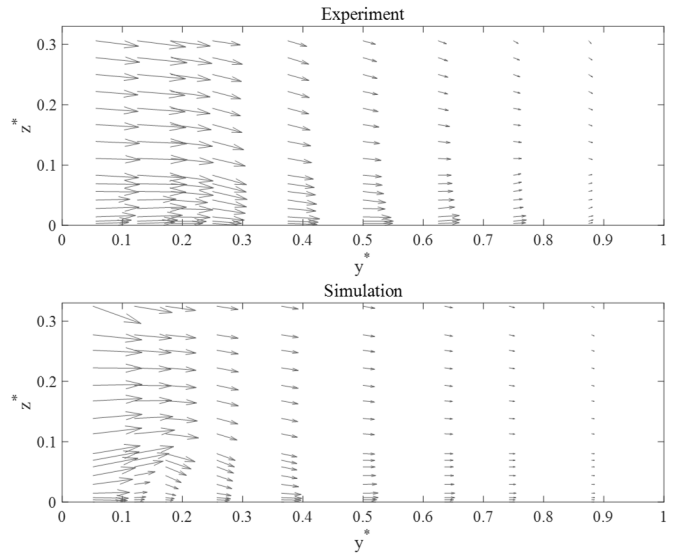

x*=2

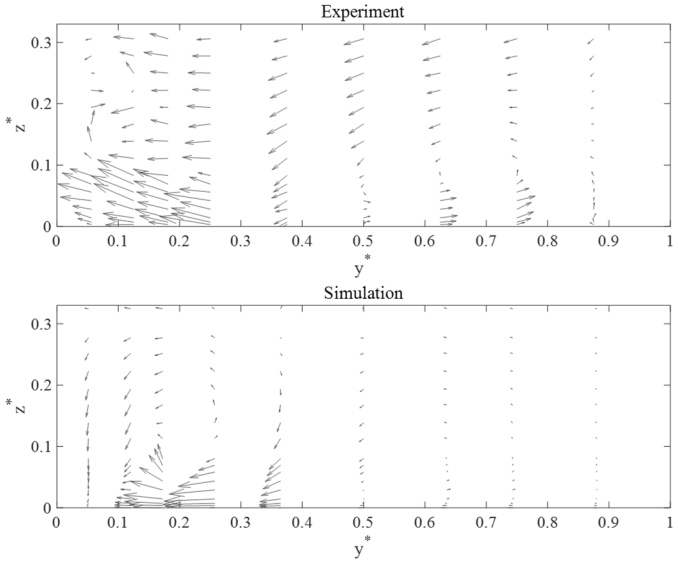

x*=3

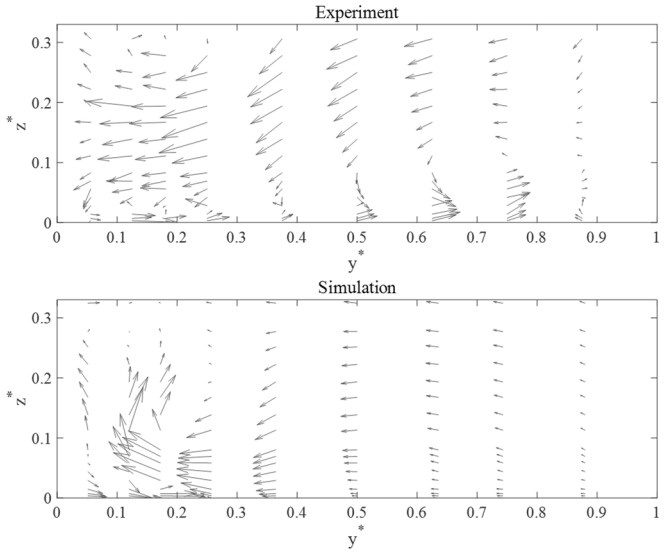

x*=5

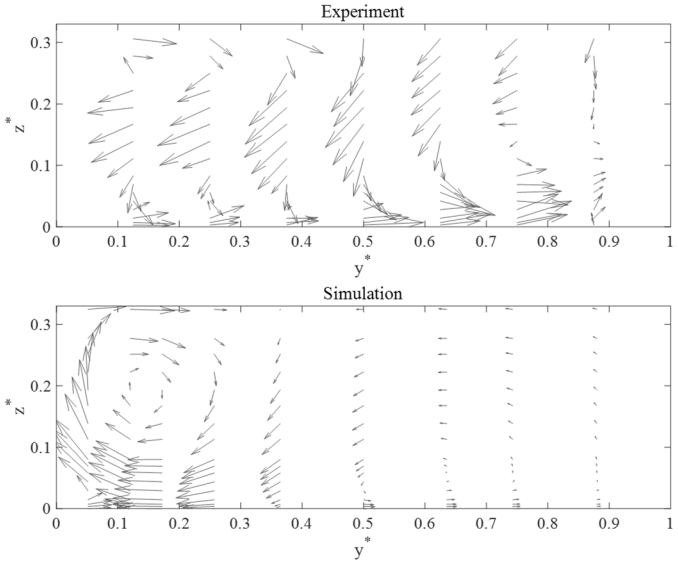

x*=7

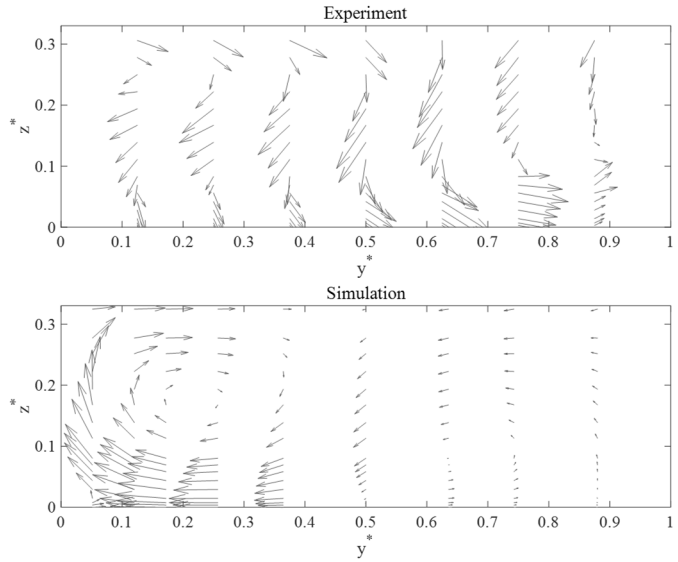

q* = 0.75

x*=0

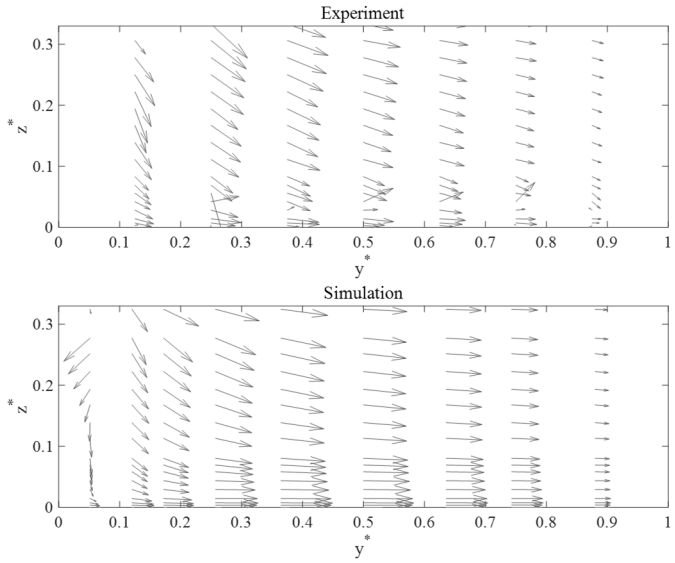
Experiment
Simulation
z*
y*
0
0.1
0.2
0.3
0.4
0.5
0.6
0.7
0.8
0.9
1

x*=1

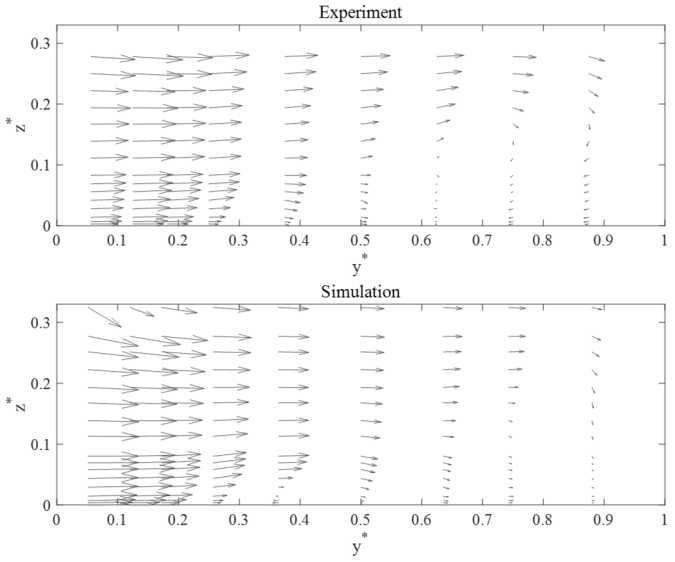
Experiment
Simulation
z*
y*
0
0.1
0.2
0.3
0.4
0.5
0.6
0.7
0.8
0.9
1

x*=2

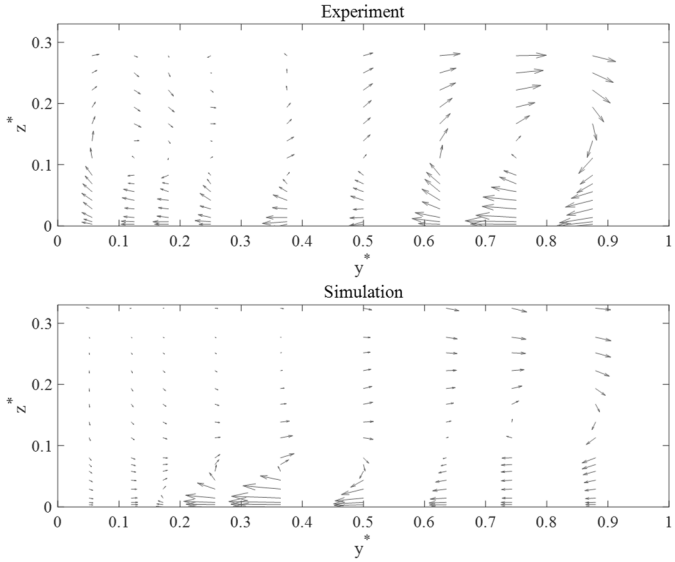
Experiment
Simulation
z*
y*
0
0.1
0.2
0.3
0.4
0.5
0.6
0.7
0.8
0.9
1

x*=3

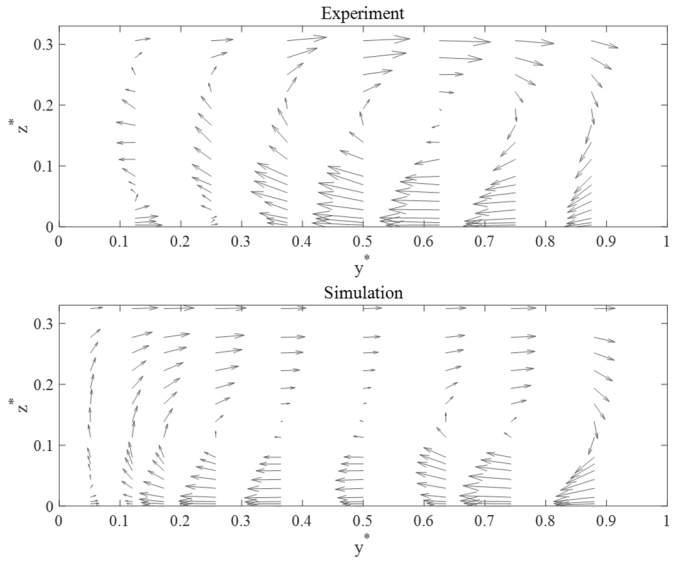
Experiment
Simulation
z*
y*
0
0.1
0.2
0.3
0.4
0.5
0.6
0.7
0.8
0.9
1

x*=5

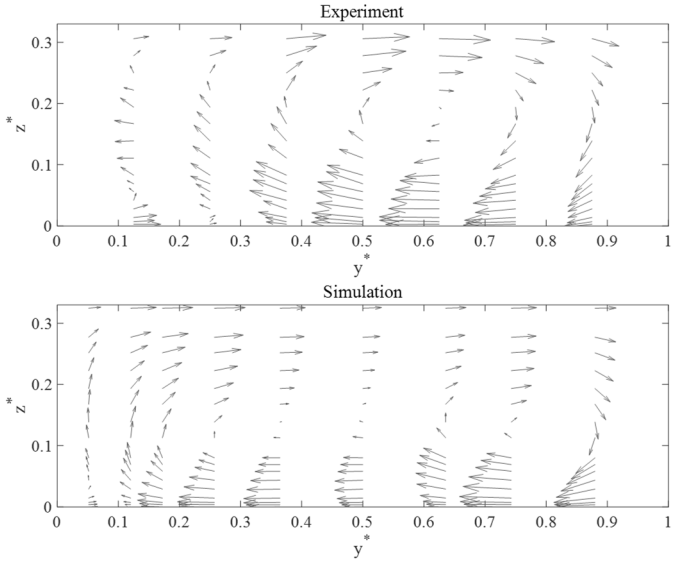
Experiment
Simulation
z*
y*
0
0.1
0.2
0.3
0.4
0.5
0.6
0.7
0.8
0.9
1

x*=7

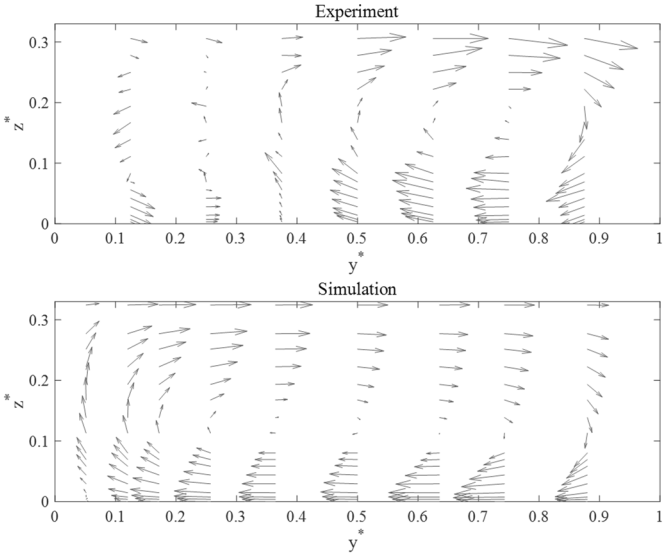
Experiment
Simulation
z*
y*
0
0.1
0.2
0.3
0.4
0.5
0.6
0.7
0.8
0.9
1

Appendix B. v*-w* vector plots of simulation of Gurram et al. (1997)

q* = 0.25, 30 degrees

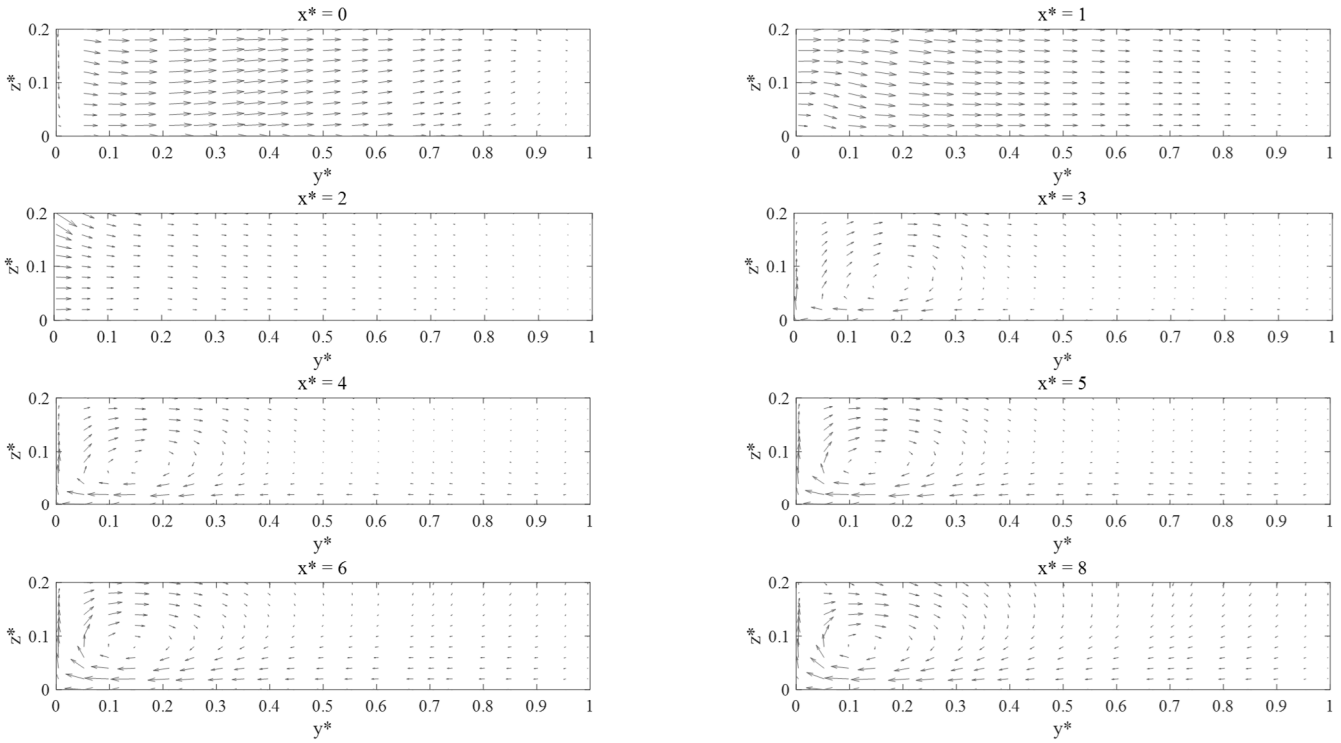

q* = 0.25, 60 degrees

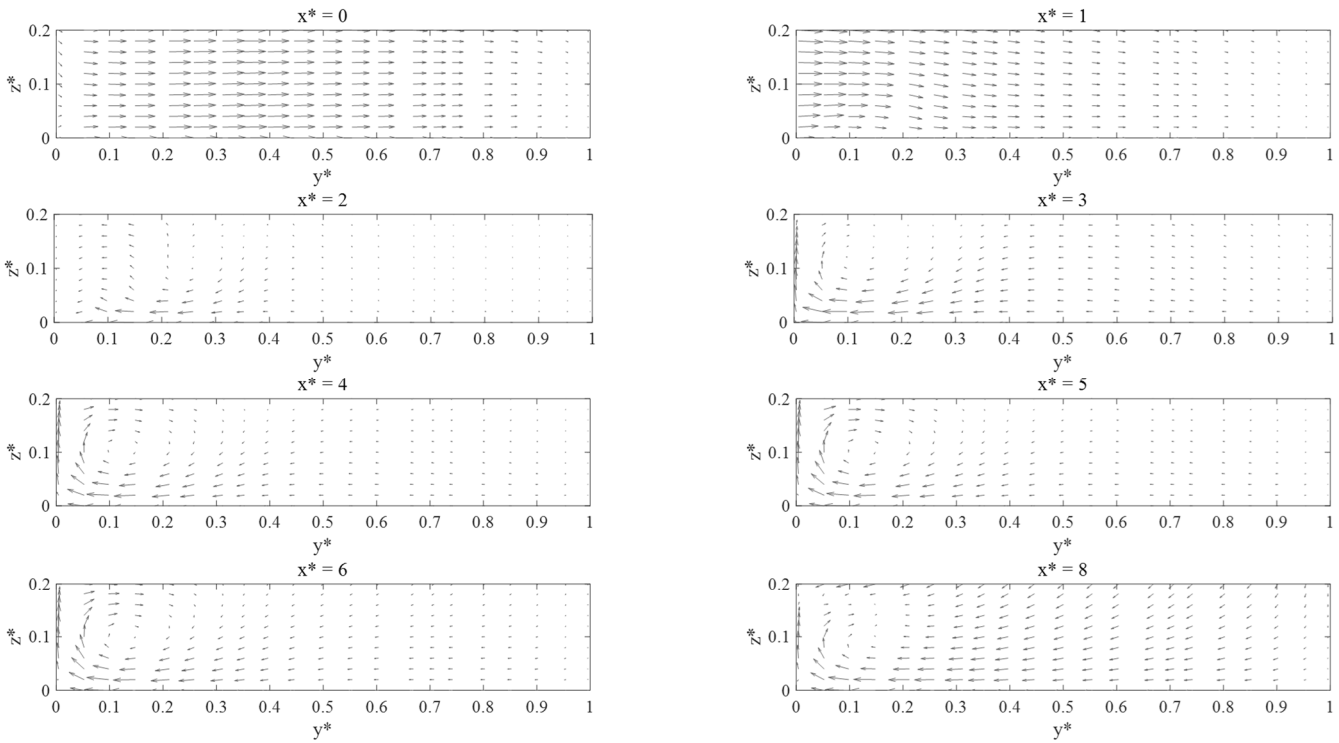

q* = 0.25, 90 degrees

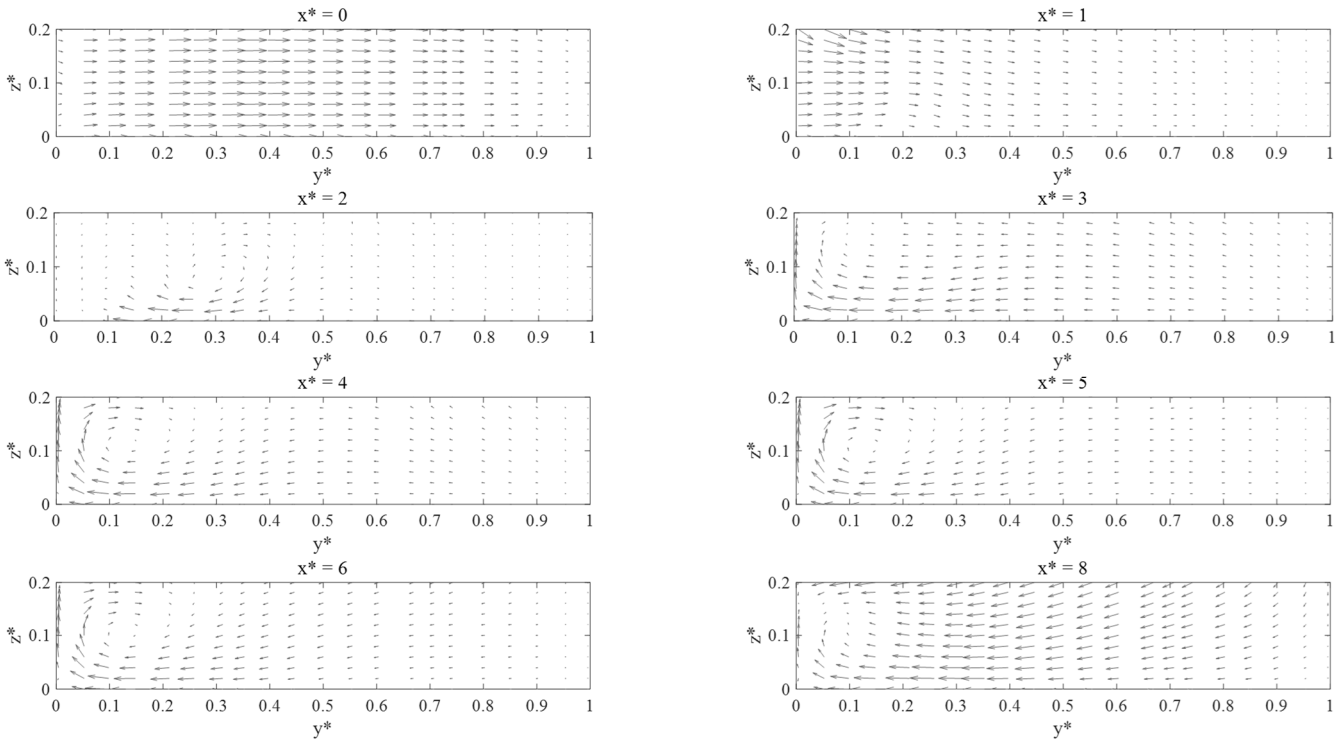

q* = 0.5, 30 degrees

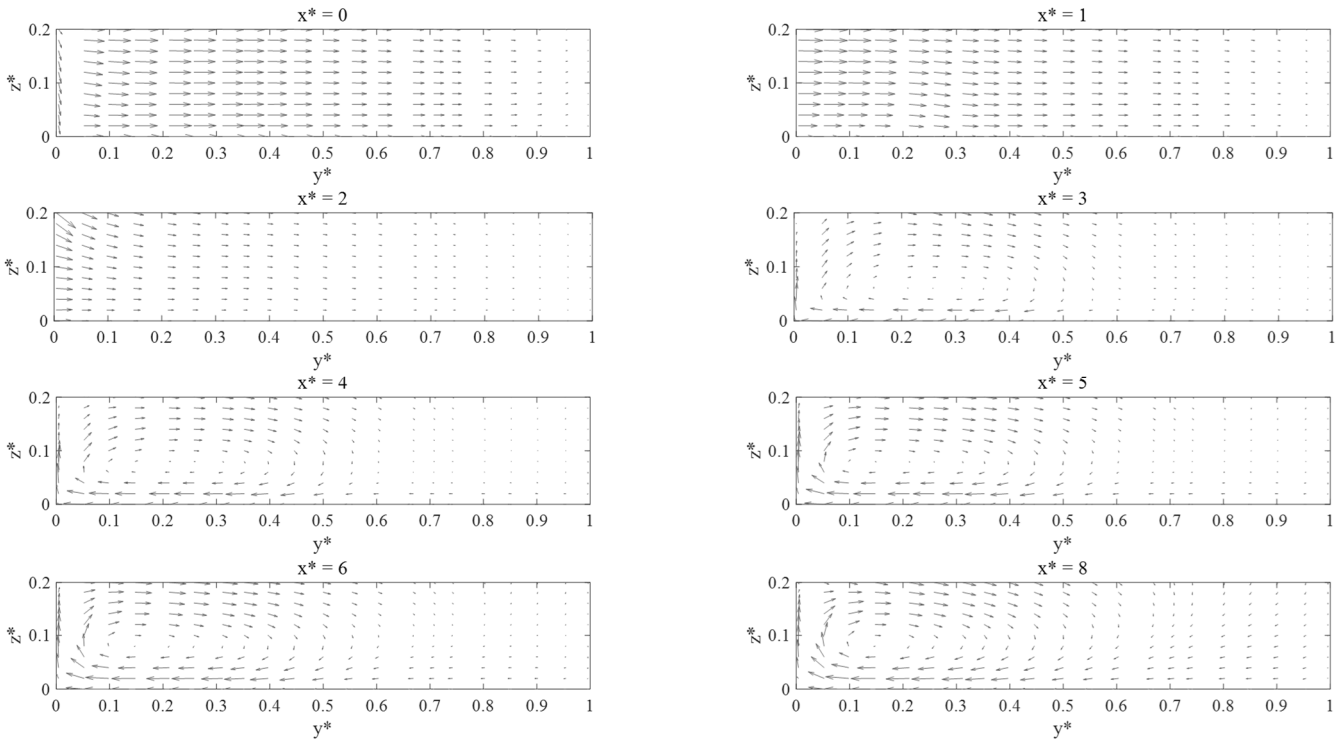

q* = 0.5, 60 degrees

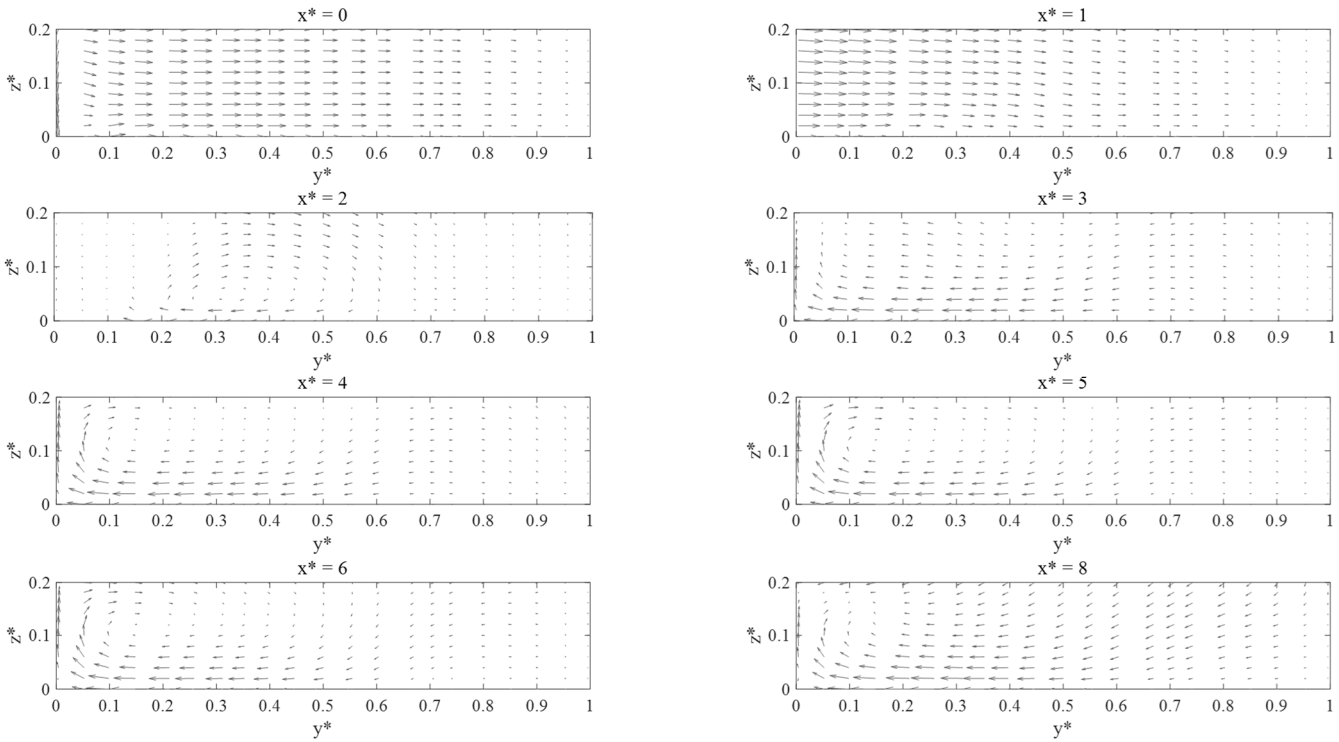

q* = 0.5, 90 degrees

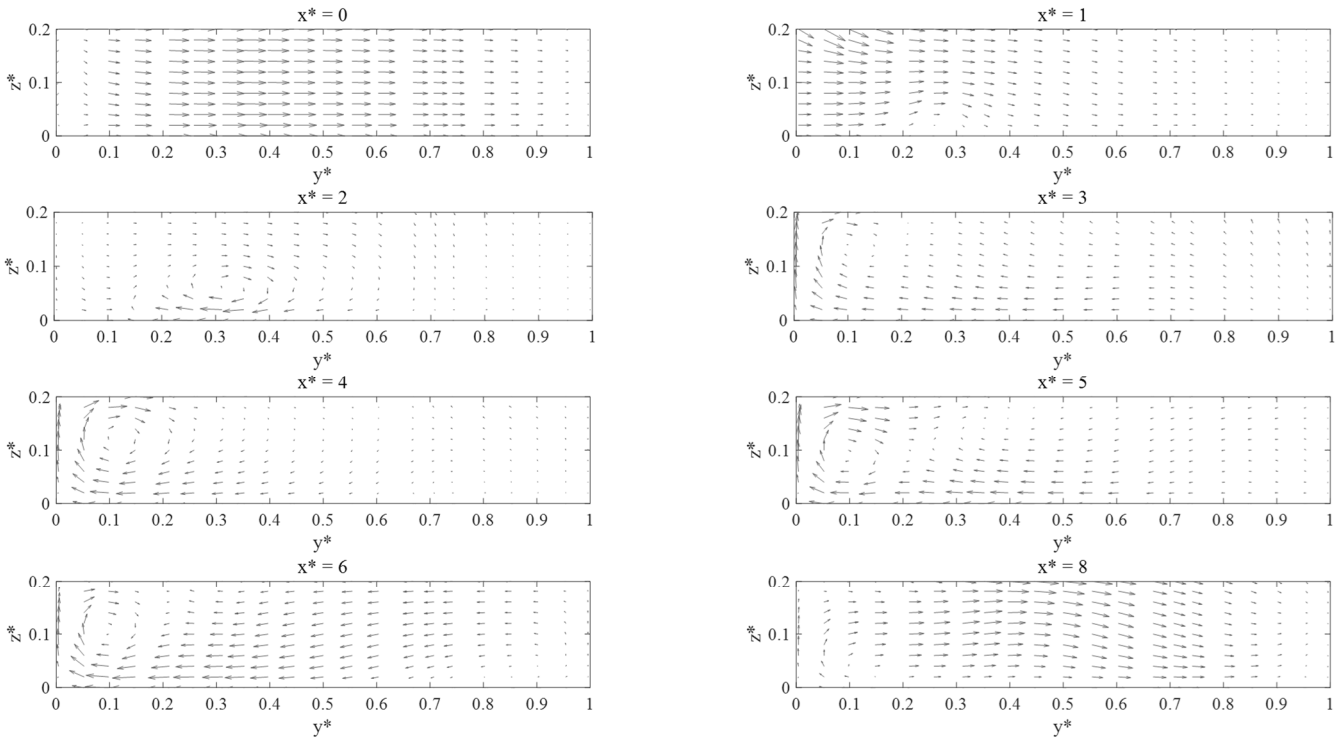

q* = 0.75, 30 degrees

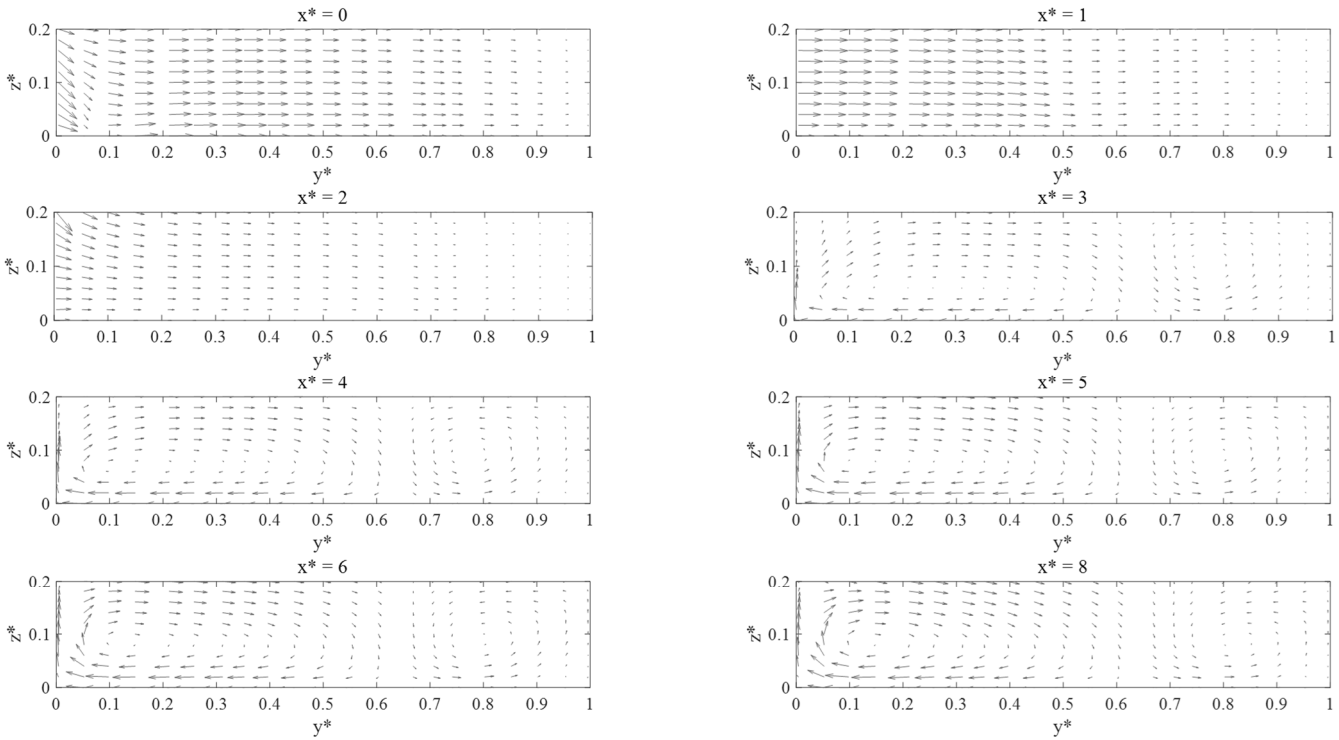

q* = 0.75, 60 degrees

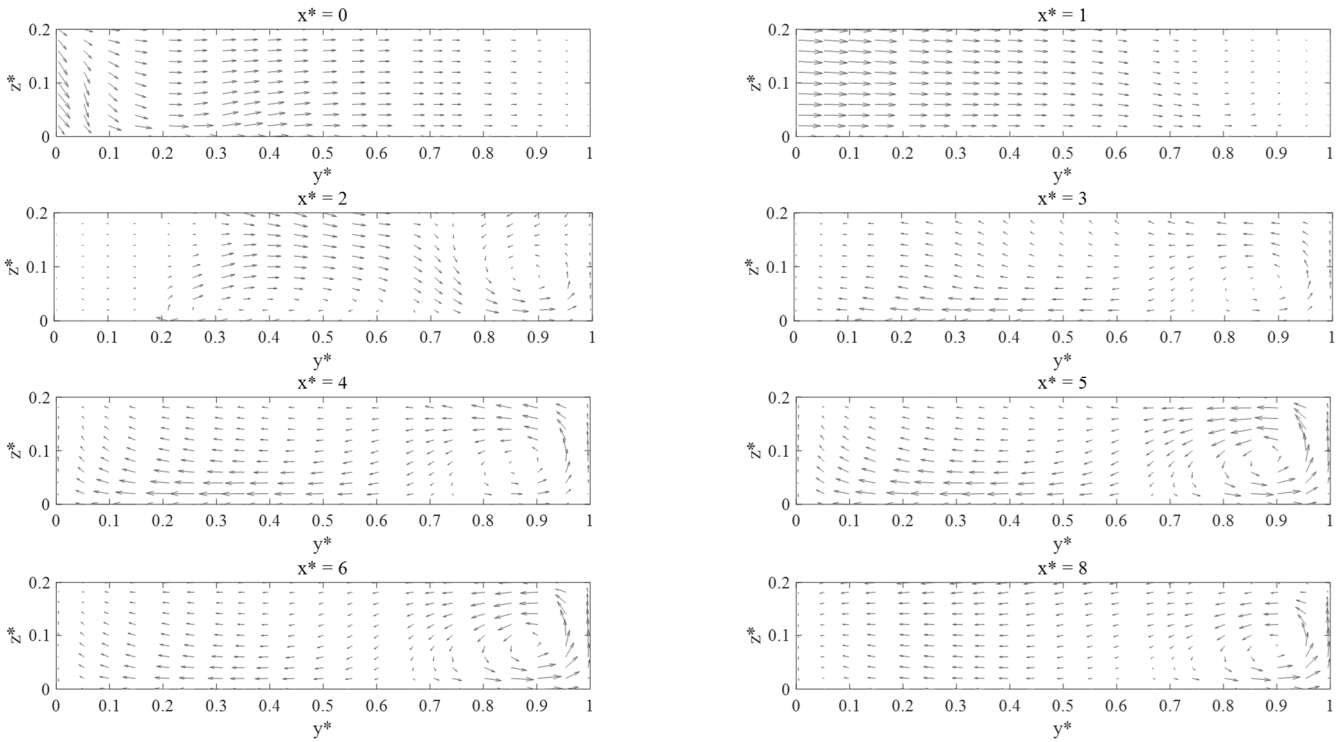

q* = 0.75, 90 degrees

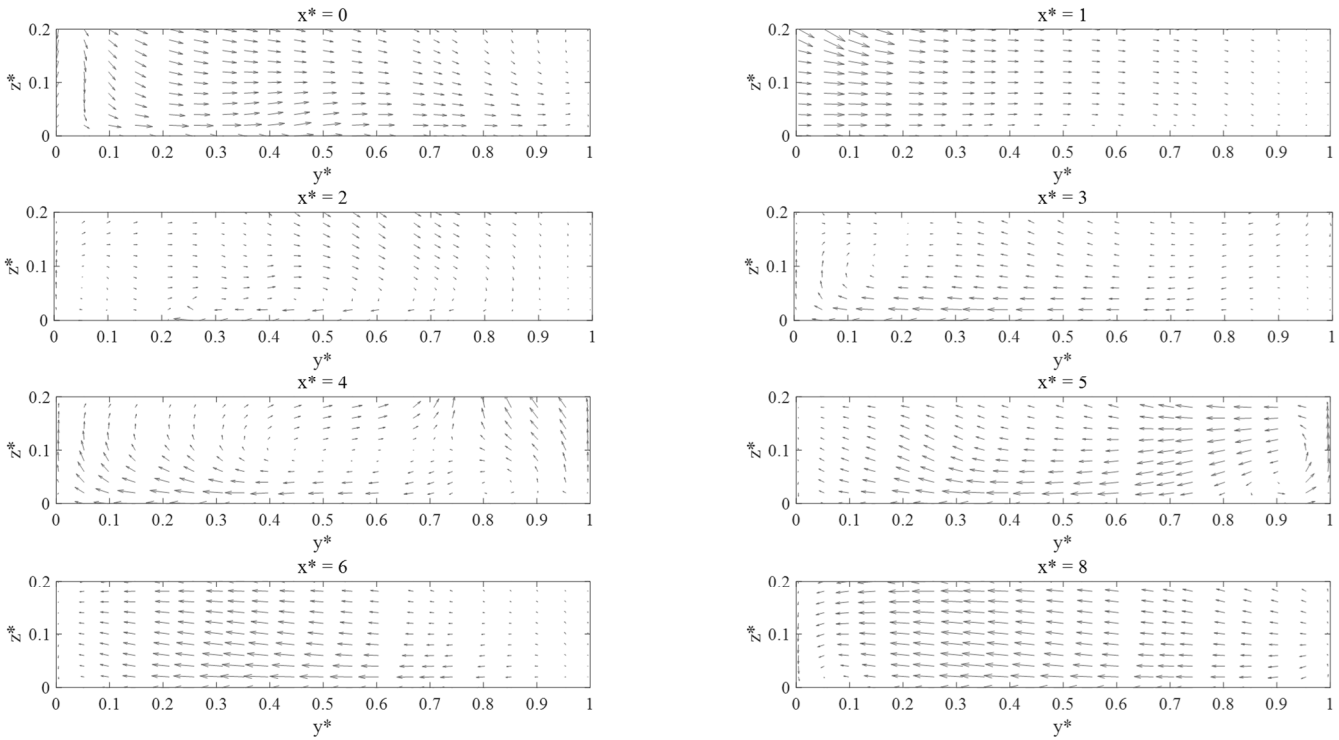

초 록

합류부 흐름은 가장 흔하고 복잡한 수리학적 현상 중 하나로, 유사이동, 하상변동, 하 · 폐수 혼합 등, 주변 환경 및 구조에 큰 영향을 주고 홍수 등의 자연재해를 일으켜 극심한 인명피해까지 야기할 수 있다. 그로 인해 다양한 분야에서 실험적뿐만 아니라 수치적으로 많은 연구의 대상이 되어왔다. 하지만 현재까지 이루어진 대부분의 수치모의는 제한적인 유량비나 접근각도에 대해서만 수행되었고 다양한 유동 특성에 대한 깊이 있는 검증은 찾아보기가 어렵다.

본 연구에서는 합류부의 각도와 유량비에 따른 합류부 흐름을 오픈소스 프로그램인 OpenFOAM을 이용하여 3차원 수치모의를 수행하였고 일차 흐름, 이차 흐름, 유동분리, 난류운동에너지, 바닥전단응력, 수심변화 등을 도식화 및 검증하였다.

모의 결과를 Gurram at el. (1997) 과 Shumate (1998)의 실험결과와 검증한 결과, 높은 부합성을 보였으며 유량비 및 접근각도가 증가할수록 대부분의 흐름특성이 증가함을 확인할 수 있었다.

모의결과로부터 다중선형회귀 모델을 도출하였고 조정결정계수와 평균제곱오차를 통해 모델의 높은 적합도와 예측력을 보여주었다. 민감도 분석 결과, 분리구역은 접근각도에, 나머지 특성들은 유량비에 더욱 민감하게 변화하는 것이 확인되었다.

하지만, 본 연구에서는 3차원 수치모의의 긴 계산소요시간 때문에 수로의 폭 및 수심은 고려하지 못했고, 실험 조건과 실험 자료에 제한이 있었기 때문에 향상된 연구의 검증 및 타당성을 위해서는 다양한 지형조건에 따른 실험을 토대로 추가적인 모의가 필요하다고 사료된다.

주요어: 합류부, 3차원 수치모델링, 유량비, 접근각도, OpenFOAM, 분리구역, 이차류.

학번: 2018-21243